Solving METHane fluxes at northern latitudes using atmospheric and soil EO data (MethEO)

Final Report

Derivable document: 5

ESRIN contract number: 4000125046/18/I-NB

Issue / Revision: 1 / 0

Date: 27 March 2020

Prepared by

Tuula Aalto, Hannakaisa Lindqvist, Aki Tsuruta, Maria Tenkanen, Tomi Karppinen, Ella Kivimäki, Tuomo Smolander, Vilma Kangasaho, Kimmo Rautiainen

Finnish Meteorological Institute (FMI)

ESA Technical Officer: Christian Retscher

FINNISH METEOROLOGICAL INSTITUTE

This page is intentionally left blank.

ESA STUDY CONTRACT REPORT

ESRIN CONTRACT NO: 4000110973/14/NL/FF/lf	SUBJECT: Solving METHane fluxes at northern latitudes using atmospheric and soil EO data (MethEO)		CONTRACTOR: Finnish Meteorological Instute, FMI
ESA CR ( )NO:	STAR CODE:	No of volumes: 1 This is volume no: 1	CONTRACTOR'S REF:

ABSTRACT:

This document forms Final Report of the project Solving METHane fluxes at northern latitudes using atmospheric and soil EO data (MethEO; ESRIN contract No. 4000125046/18/I-NB).

The main objectives of the project were to identify the magnitude of biospheric CH_4 emissions in northern high latitudes, provide global trend analysis of the methane emissions during recent decades, and identify changes in the annual cycle of CH_4 emissions, focusing on soil freeze/thaw periods. This study combined use of Earth Observation data (retrievals of atmospheric methane obtained from GOSAT and S5P-TROPOMI satellites and global soil F/T estimates from ESA Soil Moisture and Ocean Salinity Mission), atmospheric inversion modelling of methane emissions (Carbon Tracker Europe - CH_4) and ground based in situ data.

Satellite soil freeze/thaw data and methane column data, in addition to ground-based methane concentration data, were successfully utilised in atmospheric inverse modelling. The global total emissions of methane ranged between 526-561 ± 72 Tg CH_4 yr^{-1}, varying little between approaches utilising satellite data and ground-based data. The biospheric share of global emissions was 24-30%. Two major northern high latitude wetland regions were sources of 5.3 - 11.1 Tg CH_4 yr^{-1}(Western Siberian Lowlands in Russia), and 3.2 - 5.6 Tg CH_4 yr^{-1} (Hudson Bay Lowlands in Canada).

Approach utilising GOSAT satellite column data indicated higher biospheric emissions at northern latitudes than those utilising ground-based data, but evaluation against in situ measurements suggested overestimation and possibly latitudinal bias in retrievals. TROPOMI inversions suggested lower global and northern latitude emissions but showed no clear month-to-month variation in summer, suggesting a seasonal bias in retrievals. This seasonal bias was quantified for satellite column CH_4 evaluation against ground-based data. Constraining the inversion priors with soil F/T data resulted in better match of posteriors with in situ measurements. Thus, use of soil F/T data in atmospheric inversions can be recommended. The resulting annual biospheric emissions were slightly smaller (< 0.5 Tg CH_4 yr^{-1}) for northern latitudes than earlier estimations.

The estimated average trend over 2000-2018 from CTE-CH_4 inversions showed an increase in global total emissions, mostly associated with the increase in anthropogenic emissions, while the trends in global total biospheric emissions were weak and appeared positive according to the GOSAT inversion and negative according to surface inversions. In two regions in northern Siberia, the start date of the soil freezing period had a significant increasing trend, while the end date remained relatively unchanged. This implies that the total length of the soil freezing period becomes shorter. However, based on results for northern Siberia, the trends in freezing period emissions were mostly insignificant. During the soil freezing period, the methane fluxes decreased when the air and soil temperatures approached zero, and were finally retained in low winter level. The freezing period emissions ranged from 0.55 to 1.24 Tg CH_4 yr^{-1} in northern latitudes, the higher end being given by GOSAT satellite inversion and lower end by inversions utilising ground-based concentration data.

AUTHORS: Tuula Aalto, Hannakaisa Lindqvist, Aki Tsuruta, Maria Tenkanen, Tomi Karppinen, Ella Kivimäki, Tuomo Smolander, Vilma Kangasaho, Kimmo Rautiainen

ESA Study Manager: Christian Retscher	ESA BUDGET HEADING

This page is intentionally left blank.

Document change log

Issue/ Revision	Date	Observations
1.0	27-Mar-2020	First issue

This page is intentionally left blank.

Table of Contents

1 Introduction

This document describes the results of the project Solving METHane fluxes at northern latitudes using atmospheric and soil EO data (MethEO), performed within the ESA contract 4000110973/14/NL/FF/lf.

The project work is comprised of 5 tasks listed below:

Task 1. *Survey of existing data* including the following work: a survey of data sources supporting the proposed work such as EO products relevant for the CH_4 emissions in northern latitudes (retrievals of column CH_4, soil freezing and thawing information); in situ data (CH_4 fluxes and concentrations, TCCON atmospheric column observations); and possible other potential data sources. **(Deliverable D1, Existing Datasets)**

Task 2. *Dataset Collection* including the following work: the collection and consolidation of relevant Earth Observation data and data products as well as ground-based and in situ data identified and selected in Task 1 (**Deliverable D2, Dataset User Manual, and Data1, Consolidated Dataset)**

Task 3. *Development and Evaluation of Methods* including the following work: development of the methods for the estimation of the annual CH_4 emissions in the Northern Hemisphere based on using a CTE-CH_4 global atmospheric methane inversion model and the EO data; extending the SMOS based F/T product historically using another satellite based Freeze-Thaw Earth System Data Record (FT-ESDR) provided by the National Snow and Ice Data Centre (NSDIC). (**Deliverable D3, Development and Evaluation Report)**

Task 4. *Demonstration* including the following work: demonstration of the methods developed in Task 3 both at the hemispherical scale and for the case study region; trend analysis on methane emissions for a selected Eurasian region. (**Deliverable D4 Demonstration Report**)

Task 5. *Impact Assessment and Scientific Roadmap* including the following work: analysis of the scientific impact of the developed products and the applicability of the developed and improved methods and products beyond the demonstration purposes performed during Task 4. **(Contribution to Deliverable D5, Final Report**)

2 Overview and Results

2.1 Task 1: Survey of existing data

The objective of Task 1 was to survey and describe the existing datasets that are utilized in the project for the intensive case study, performed during the project, and for the inverse modelling with CarbonTracker-Europe CH_4 (CTE-CH_4) model. Work included (1) survey of Earth Observation (EO) data sets; and (2) in situ data relevant for the study; and (3) comparison of three commonly used Greenhouse Gases Observing Satellite (GOSAT) CH_4 retrievals (NIES, RemoTeC CH_4 -Full Physics and RemoTeC CH_4 Proxy) concerning the data availability and retrieval uncertainties.

2.1.1 Survey of Earth Observation (EO) data sets

In the proposal, two EO products were listed as a baseline for this study: GOSAT column-averaged methane concentrations (XCH_4) and SMOS freeze and thaw (F/T) retrievals. During the project, TROPOMI XCH_4 observations have become available and those have been evaluated and included in the study.

2.1.2 Survey of in situ CH_4 measurements

Based on (1) the survey of in situ flux and concentration sites, and (2) high latitude location with clearly distinct seasons and large wetland areas, northern Fennoscandia (area over northern Finland, Sweden and Norway) was selected as an intensive case study region. The region includes many in situ flux and concentration sites with long time series required for the MethEO project. Locations of these sites are shown in Figure 1.

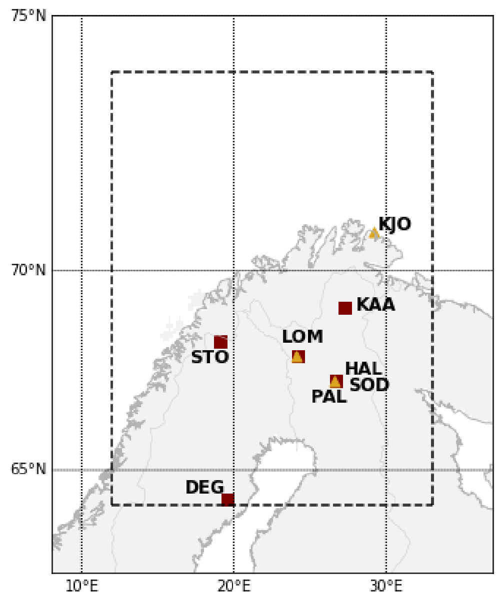

Figure 1: In situ sites at the northern Fennoscandia in the study region, yellow triangles refer to the in situ concentration sites and red squares refer to the in situ flux sites. The area marked by dashed lines shows the case study area for which CH_4 fluxes are optimised in a grid size of 1° x 1° in CTE-CH_4.

2.1.3 Comparison of different GOSAT CH_4 retrievals

Three different XCH_4 retrieval products for GOSAT observations were compared against ground based TCCON observations (Wunch et al., 2011): NIES v02.72 (Yoshida et al. 2013), RemoTeC Full Physics v2.3.8 (Detmers, 2016a), and RemoTeC Proxy v2.3.8 (Detmers, 2016b). The comparison results are shown in Figure 2 and Table 1.

The uncertainties of the three GOSAT retrieval algorithms are of similar orders of magnitude. The retrievals differ notably in the data coverage for the study region: the RemoTeC Proxy retrieval has considerably more data compared to the other two retrievals. RemoTeC Full Physics had the least data.

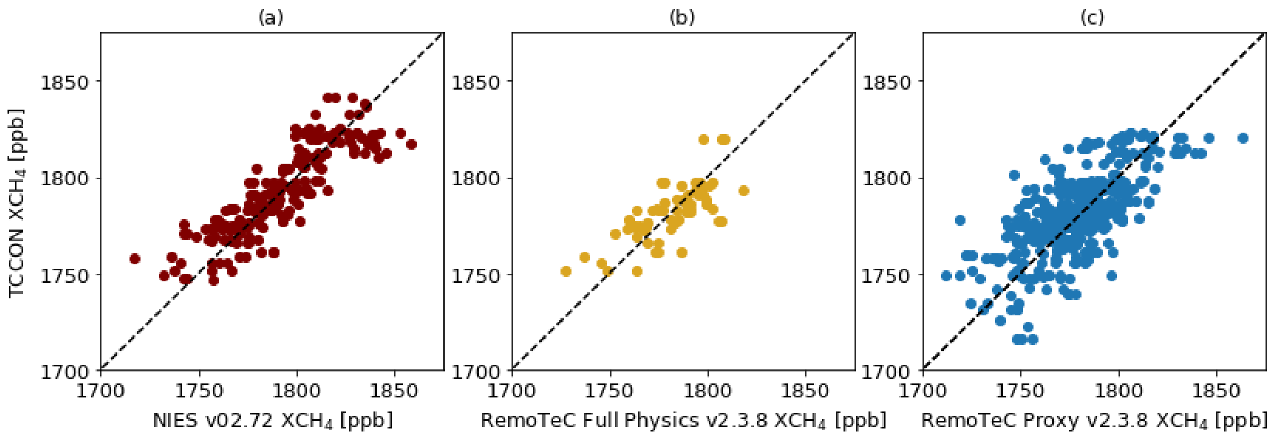

Figure 2: Comparison of the TCCON and GOSAT observations against one-to-one line. Co-location criteria for the GOSAT observations were ±2 °from the TCCON site in longitude and latitude, and the TCCON observations were considered within ±30 min from the GOSAT overpass.

Table 1: Calculated biases and standard deviations for Sodankylä TCCON site, calculated as GOSAT XCH_4 – TCCON XCH_4. Spatial co-location criteria for GOSAT observations were ±2 °in latitude and longitude from the TCCON site, and the TCCON observations were considered within ±30 min from the GOSAT overpass.

Retrieval method	N	Bias [ppb]	σ [ppb]	Time series
NIES v2.72	196	-1.30	13.51	April 2009 – September 2017
RemoTeC Full Physics v2.3.8	67	-0.94	12.46	June 2009 – August 2015
RemoTeC Proxy v2.3.8	420	-2.42	17.22	June 2009 – September 2015

2.1.4 Evaluation of TROPOMI XCH_4 retrievals at Sodankylä

The total column methane (XCH_4) product from Sentinel 5-P TROPOMI (launched in October 2017) became available during the duration of the project. We evaluated the product against the ground-based FTS in Sodankylä that participates the TCCON (Kivi and Heikkinen, 2016). Co-location criteria were ± 2° from the TCCON site in longitude and latitude, and same-day soundings were considered.

The co-located TROPOMI XCH_4 and TCCON XCH_4 time series are presented in Figure 3. The comparison reveals that TROPOMI has an overall low bias as compared to the TCCON. An important finding is that the bias is not constant but depends strongly on season, varying up to roughly 60 ppb within a year. While the agreement is good in the early months in spring, towards the autumn the differences increase notably. We have carried out investigations on the potential reasons for this bias, and evaluated the effect of snow-covered surfaces and the polar vortex, both of which are known to affect XCH_4 retrievals from space. These are identified in Figure 3. Thus far, the source of the seasonal bias remains inconclusive.

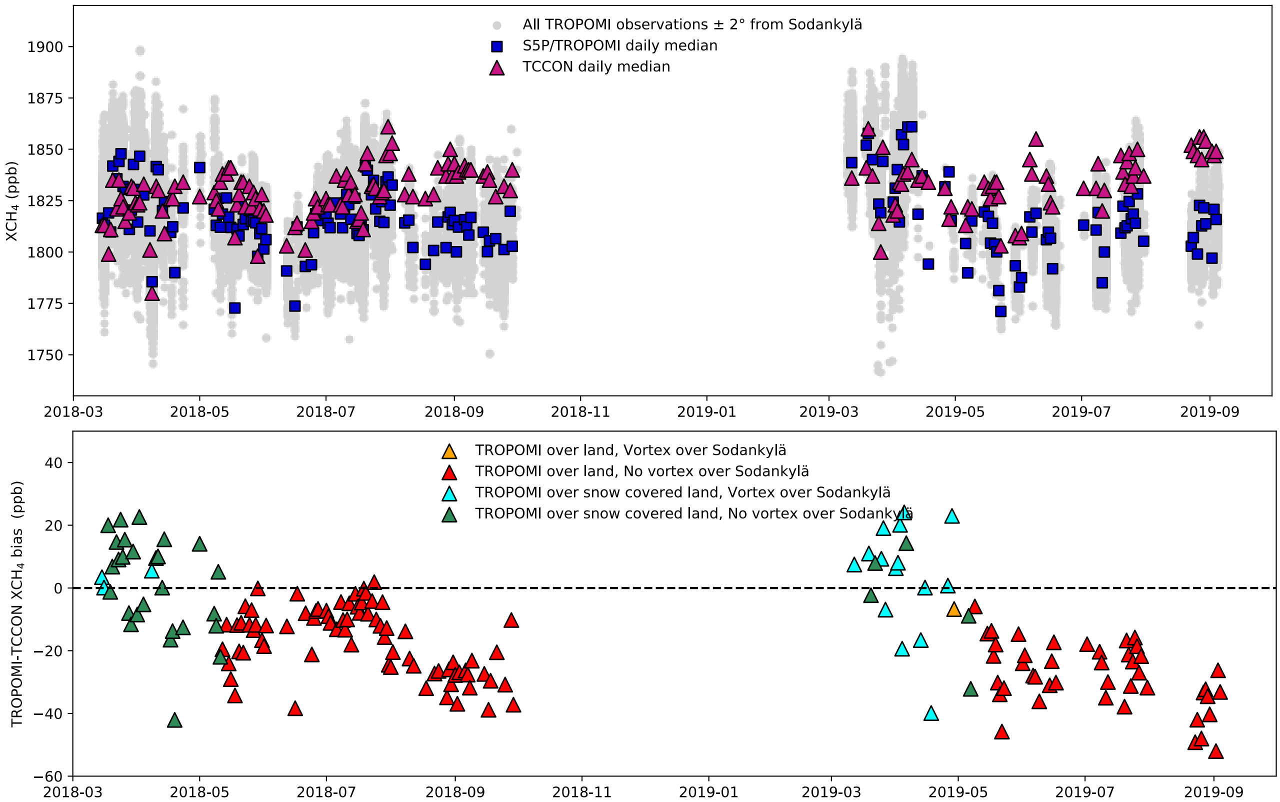

Figure 3. Evaluation of Sentinel 5-P TROPOMI XCH_4 product against TCCON at Sodankylä. Upper panel: Time series of co-located observations; Lower panel: bias calculated from the daily medians (TROPOMI XCH_4 – TCCON XCH_4) and color-coded based on polar vortex conditions and/or snow coverage.

2.2 Task 2: Dataset Collection

The objective of Task 2 was to collect and consolidate all data relevant for the study based on the outputs from Task 1 (Survey of existing data). The selected input data includes ground-based in-situ (CH_4 flux, concentration and total column measurements) and EO data (GOSAT and TROPOMI XCH_4 retrievals and SMOS based F/T retrievals). A summary of these data and their temporal coverage and spatial resolution is presented in Figure 4. Detailed information on selected in-situ concentration and flux site time series are given in Table 2.

The project output product, CTE-CH_4 fluxes, is also provided in a consolidated data package to ESA. The output deliverables include Dataset User Manual and Consolidated Dataset. In Dataset User Manual all used data are described in detail.

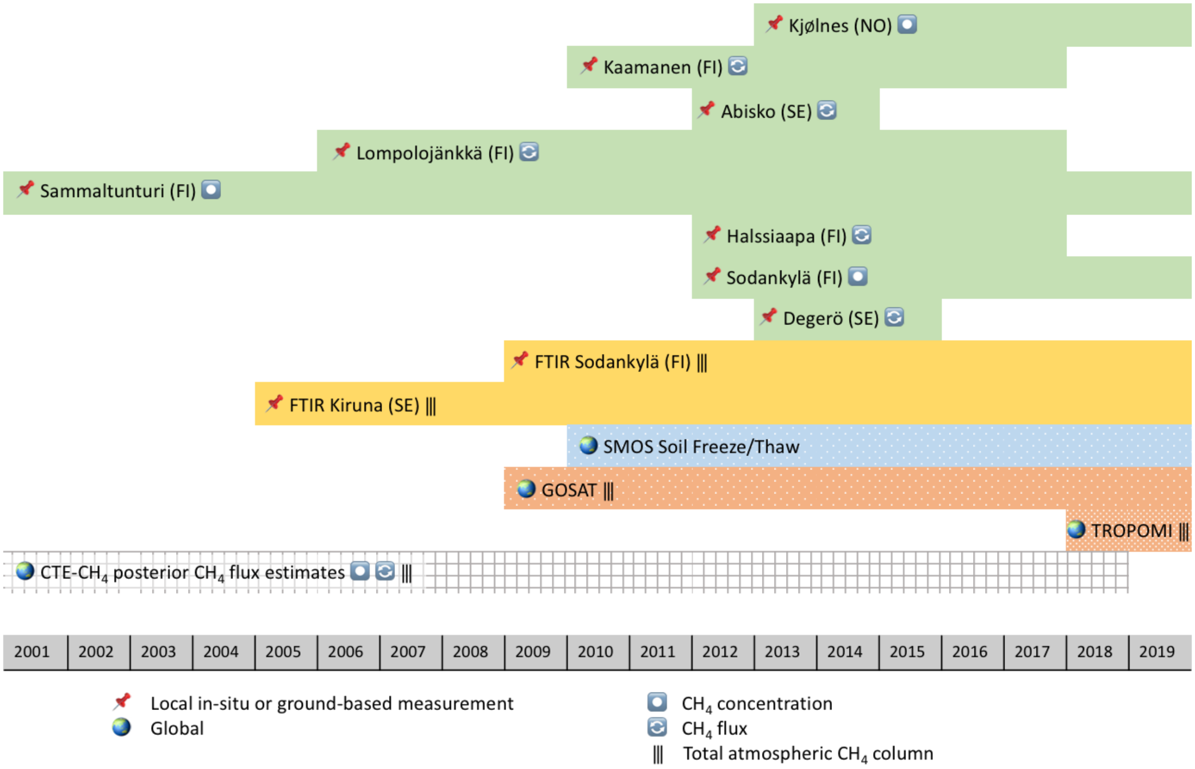

Figure 4. Summary of the essential project data: ground-based in-situ (green) and remote sensing (yellow) measurements, SMOS Soil Freeze/Thaw satellite product (blue), satellite retrievals of CH_4 (orange), and the project output CTE-CH_4 product.

Table 2: Detailed information about the in-situ concentration and flux site time series. The sites are organised from the northernmost site (Kjølnes) to the southernmost (Degerö).

Site name	Short	Flux/Concentration	Time series	Site location	Operated
Kjølnes (NO)	KJO	Concentration	08/2013 →	70.85° N, 29.24° E	Exeter
Kaamanen (FI)	KAA	Flux	07/2010 – 12/2017	69.14° N, 27.27° E	FMI
Abisko-Stordalen (SE)	ABI	Flux	06/2012 – 12/2014	68.35° N, 19.05° E	SPRS
Lompolojänkkä (FI)	LOM	Flux	08/2006 – 12/2017	68.0° N, 24.21° E	FMI
Sammaltunturi (FI)	SAM	Concentration	02/2004 →	67.97° N, 24.12° E	FMI
Sammaltunturi (FI)	SAM	Concentration	12/2001 →	67.97° N, 24.12° E	NOAA
Halssiaapa (FI)	HAL	Flux	06/2012 – 12/2017	67.37° N, 26.65° E	FMI
Sodankylä tower (FI)	SOD	Concentration	06/2012 →	67.36° N, 26.64° E	FMI
Degerö (SE)	DEG	Flux	05/2013 – 12/2015	64.18° N, 19.55° E	SLU

2.3 Task 3: Development and Evaluation of Methods

The objective of Task 3 was to develop methods for the estimation of the annual CH_4 emissions in the Northern Hemisphere using CTE-CH_4 global atmospheric methane inversion model with the selected EO data (GOSAT, TROPOMI and SMOS F/T). CTE-CH_4 model system was developed to assimilate both in-situ measurements and EO (GOSAT and TROPOMI) total column (XCH_4) data. The in-situ surface atmospheric CH_4 observations have better measurement precision but very limited spatial coverage compared to EO data. By assimilating the EO data the spatial coverage was improved dramatically.

The CTE-CH_4 results were compared to i) direct CH_4 wetland flux observations and ii) atmospheric CH_4 at surface in situ stations and column data of the satellite in order to evaluate the performance of the inversion model.

The SMOS F/T data were utilized in building the prior estimates for the biospheric fluxes, in order to improve the seasonal cycle of the emissions in the prior. Biospheric CH_4 fluxes after the soil-freezing period were assumed to be small, until when the soil starts to thaw in spring.

Another objective of Task 3 was to extend historically the SMOS based soil F/T data (temporal coverage: 2010-present) using the FT-ESDR (the Earth System Data Record for Land Surface Freeze/Thaw State) F/T data (temporal coverage: 1980 – 2017). FT-ESDR is provided by the National Snow and Ice Data Centre (NSIDC). The extended timeseries of F/T information was used in trend analysis in Task 4.

2.3.1 Evaluation of Carbon Tracker Model Data

The existing results of the CTE-CH_4, assimilating only in situ concentration measurements (denoted here as SURF1 and SURF2), were compared to direct CH_4 wetland flux observations. SURF1 optimizes CH_4 emissions globally, and CH_4 emissions in Finland and Scandinavia have been solved in high 1° x 1° resolution. SURF1 utilises concentration data from 3 in situ stations in the focus region (Figure 1, Table 2), and ecosystem priors from LPX-Bern-DYPTOP model (Stocker et al., 2014). In SURF2, CH_4 emissions in Europe have been solved in 1° x 1° resolution. It utilizes the concentration observations and ecosystem priors provided by the Global Carbon Project 2018. There are less observations in the region of interest, and ecosystem priors are climatological, i.e. they do not change from year to year. The wetland extent is also different in the two set-ups; SURF1 prior uses wetland extent from DYPTOP model, while SURF2 prior is an average of flux estimates from various ecosystem models, having no single underlying wetland extent map.

2.3.1.1 Comparison to biospheric fluxes measured at wetland sites

In order to compare to site measurements, nine 1° x 1° grid cells surrounding the sites were extracted from the CTE-CH_4 results and an average of the biospheric fluxes were taken to represent the site emissions. The beginning and end of the freezing period was determined from both the SMOS results and meteorological data, for a large modified TransCom (mTC) region (here Finland and Scandinavia) and at the measurement sites. The freezing period is an annual time period during which the soil is freezing and thus, it excludes wintertime when the soil is frozen. For description of the mTC regions, see Figure 5. The start of the freezing period had to fulfil two conditions: in each mTC region, 1) the percent of ”frozen” grid cells had to be over 2% according to the SMOS F/T data, and 2) the average air temperature had to be lower than 2 °C according to the ERA-Interim reanalysis. The end of the freezing period was defined in a similar manner: in each mTC region, 1) the percent of ”frozen” grid cells had to be over 80 %, and 2) the average air temperature had to be under 0 °C. Air temperatures measured at the site were used to determine soil freezing period at the sites, together with SMOS soil freeze data from the area surrounding the site. The timing of soil freezing is similar within the nearby grid cells, and thus the freezing period is usually shorter at the site than in the whole mTC region (Figure 6).

Generally, the seasonal cycle of the measured fluxes and modelled fluxes agree well. However, there are some differences in the SURF1 and SURF2 results due to the different model set-ups. Generally, SURF1 appears to be performing better. Both in the observations and in the model the methane fluxes decrease when the air and soil temperatures approach zero. During the actual soil freezing period the fluxes are usually small and decrease towards the full winter state. Interestingly, during autumn 2012 at a boreal non-permafrost site Lompolojänkkä, both measurements and model show a small increase in emissions, which occurs during the local freezing period as indicated by both satellite and local temperature measurements (Figure 6). The increase is not clearly present at all measurement years and sites (Figure 7), and the permafrost areas do not show clear distinction from non-permafrost areas. However, at all sites there were both modelled and observed methane emissions during the freezing period, or 'zero curtain' period, as reported earlier by e.g. Zona et al. (2016), Arndt et al. (2019) and Mastepanov et al. (2013).

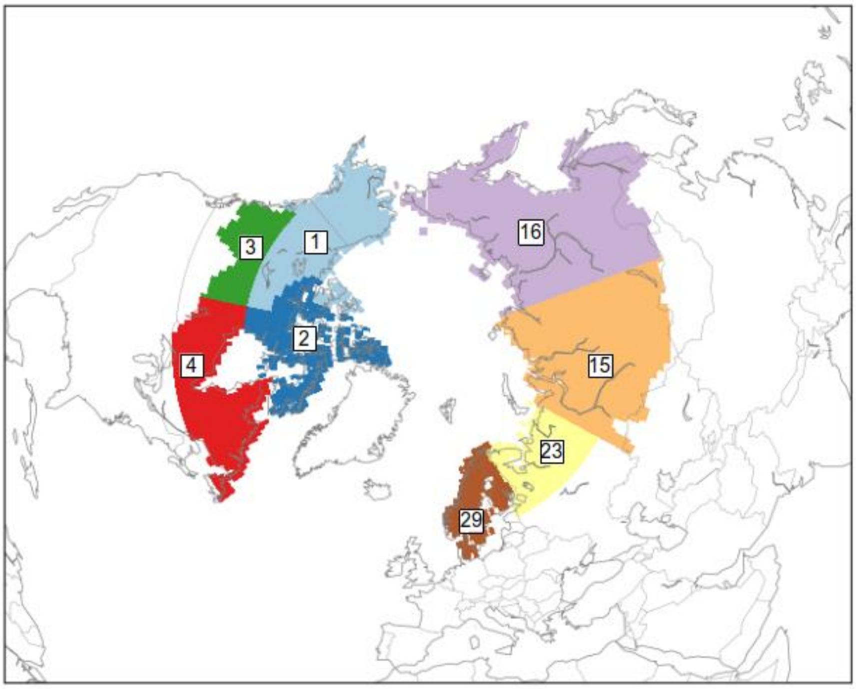

Figure 5. The northern modified TransCom (mTC) regions covered by this study.

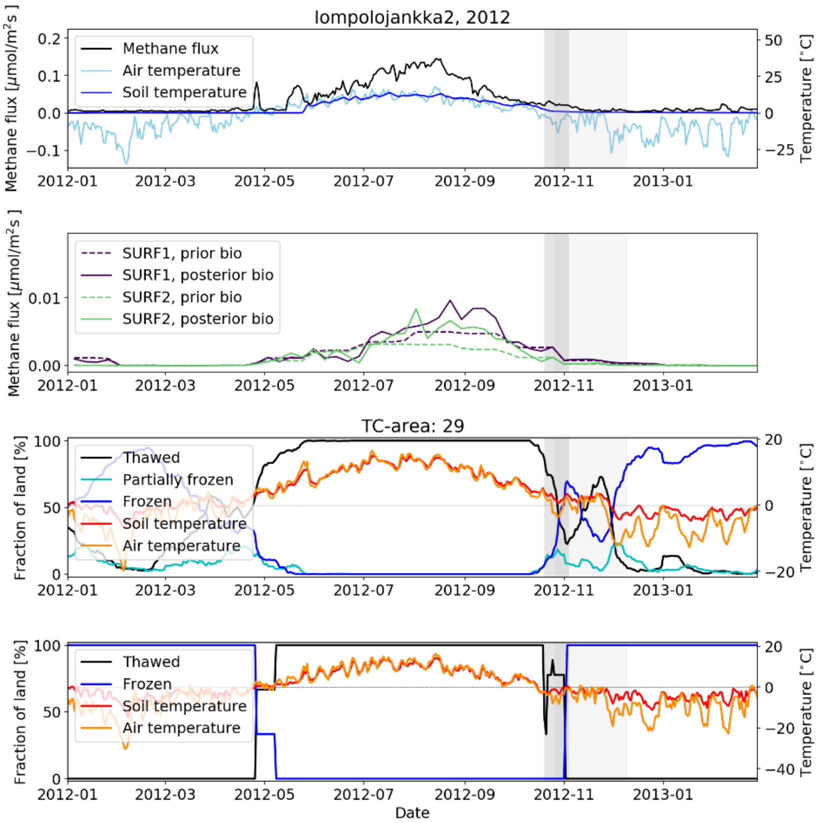

Figure 6. Comparison to site results at Pallas Lompolojänkkä, Northern Finland. Panel 1: Measured fluxes at Lompolojänkkä wetland (eddy covariance) and temperatures measured at the site, panel 2: CTE-CH_4 prior and posterior biospheric methane emissions (nine grid cells -based) according to SURF1 and SURF2 inversions, panel 3: Soil freeze in Fennoscandia according to satellite (SMOS) together with ERA-Interim temperatures, panel 4: Soil freeze in Lompolojänkkä region according to satellite (SMOS) together with ERA-Interim temperatures. The freezing period in Fennoscandia is accentuated by a light grey bar, and local freezing period by a dark grey bar.

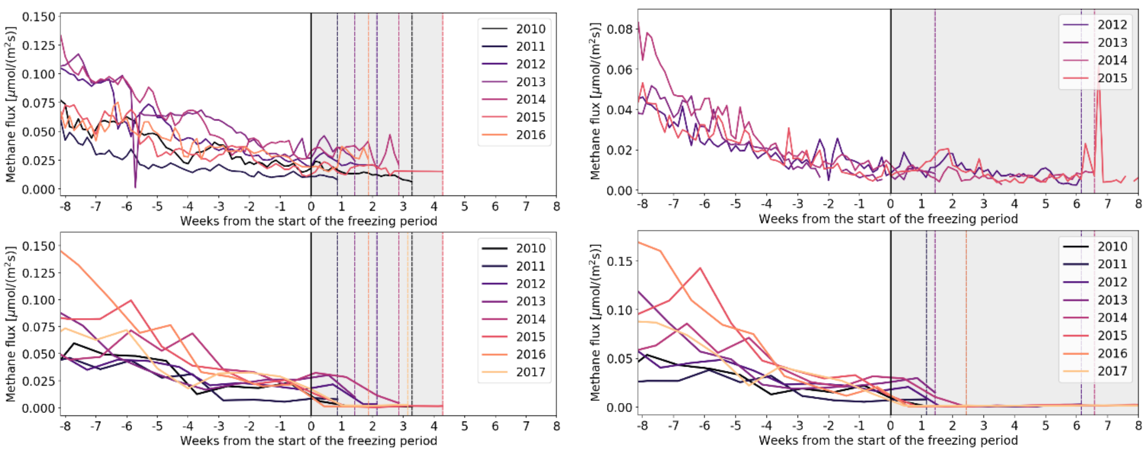

Figure 7. Comparison to site results at a) Pallas Lompolojänkkä, and b) Sodankylä Halssiaapa, Northern Finland. Panel 1: Measured wetland fluxes (eddy covariance), panel 2: CTE-CH_4 posterior biospheric methane emissions both sites according to SURF1 inversion (nine grid cells -based). The local freezing period is accentuated by light grey, and vertical lines correspond to the end of the period each year.

2.3.1.2 Correlations between modelled biospheric fluxes and freezing period length

The freezing periods were extracted from the SMOS satellite data for boreal and arctic circumpolar mTC regions (see Figure 5). The biospheric methane fluxes were extracted from the model results for the same periods. The results show a good correlation between methane fluxes and length of the freezing period, indicating that methane emissions increase when the length of the freezing period increases (Figure 8). However, the magnitude of the emissions was not significantly increased from the prior estimate suggesting that unexpectedly high emission bursts either did not occur during the freezing period, or that they were limited to local areas and/or very short periods of time, thus not being visible in the large regional inversion results. The results were similar for Eurasia and North America.

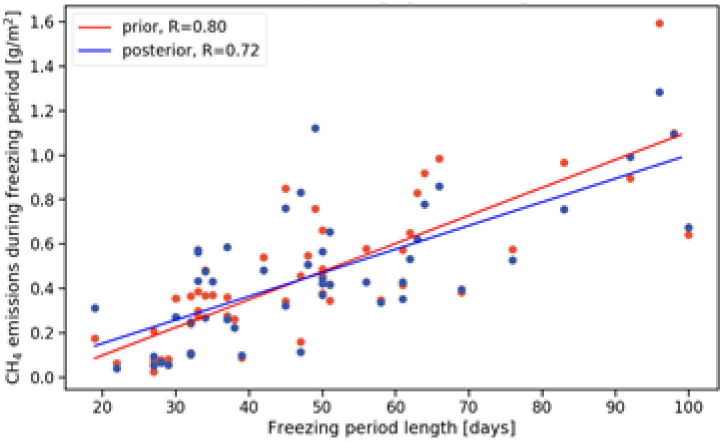

Figure 8. The methane emissions during soil freezing period in eight northern modified TransCom (mTC) regions, plotted against the length of the freezing period. Each dot refers to one mTC region and one year. The emissions are expressed per unit wetland area, because absolute magnitudes largely differ in regions with different wetland extents.

2.3.2 Extension of the SMOS F/T time series

For the trend analysis in WP400, the SMOS F/T time series were extended with global FT-ESDR (Earth System Data Record for Land Surface Freeze/Thaw State) dataset. The SMOS data are available from July 2010 onwards, FT-ESDR dataset starts from 1979 and is currently processed until the end of 2016. The two products were compared during the overlapping periods (2010-2016). For MethEO study purposes, soil F/T data are used to determine the soil freezing period for each modified TransCom (mTC) area (see Figure 5 and Section 2.3.1). The comparisons were performed for each region and for each coinciding freezing period separately. For the comparison, the number of frozen pixels in respect to total pixels were calculated. For both datasets the area was limited to only pixels where less than 10% of the dates were missing data in the SMOS product during the freezing periods (August – February) of the years 2010 – 2016 combined.

The daily variation on the FT-ESDR product estimates is significantly larger than those of SMOS F/T product estimates. Most probably due to the high operating frequency (37 GHz) on SSMI instrument used for FT-ESDR product – the measurement originates only on the very surface of the landscape and thus e.g. changes in air temperature are more likely to affect the F/T estimates. To mitigate the variation in the FT-ESDR product, a day of soil freezing was determined for each pixel as the first day that showed frozen state so that four following days were also in frozen state. After this five-day frozen period the pixel in question was determined to stay frozen for the rest of the year.

The FT-ESDR product includes information from AM and PM orbits. The satellite is in sun-synchronous orbit, AM orbit overpasses the equator around 6 AM and PM orbit around 6 PM. The air temperature is typically at local minimum close to the AM overpasses. The SMOS F/T data were compared to FT-ESDR data (a) using both AM and PM information and (b) using only AM information. The comparison results for the mTC 16 are shown in Figure 9 (using information from both AM and PM orbits) and in Figure 10 (only compared against FT-ESDR AM data). For the start of the soil freezing, the best results were achieved when using FT-ESDR data that contained information from both AM and PM orbits. However, for the end of the soil freezing period, the two datasets were most consistent if only FT-ESDR AM data were used. The results for each region are provided in Table 3, with mTC regions 15 and 16 highlighted. The most consistent results were obtained for mTC regions 15 and 16 – Western and Eastern Siberia. Therefore, these mTC regions were selected for trend analysis.

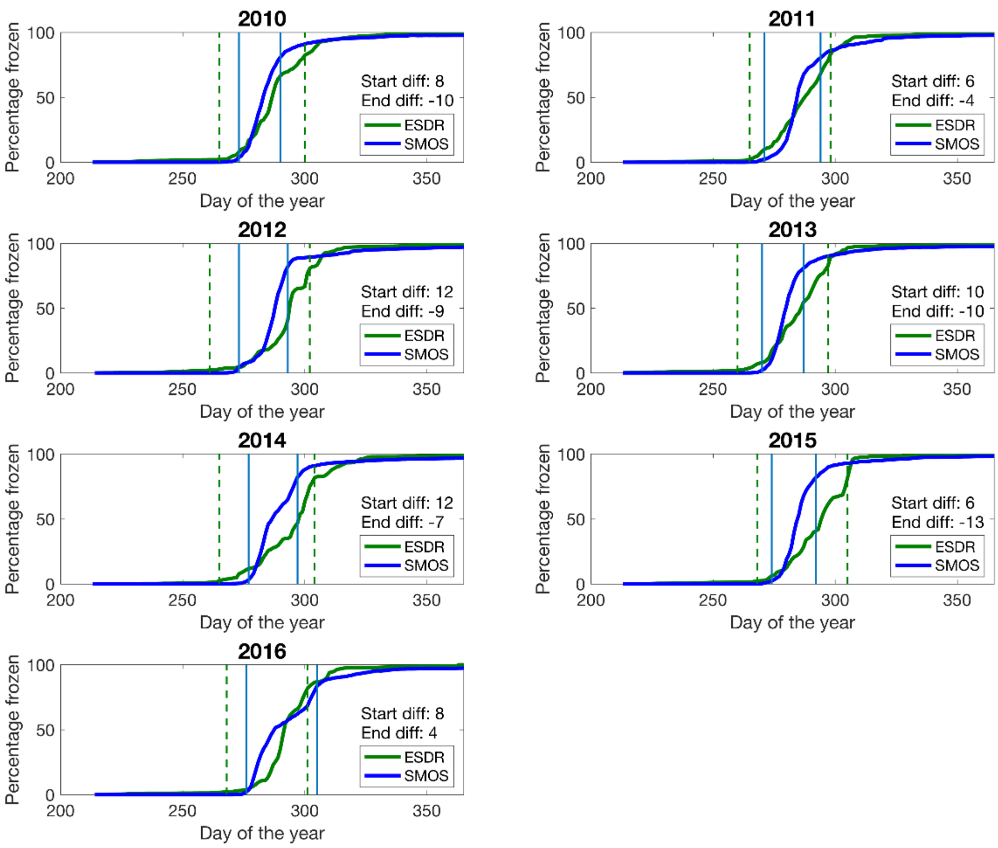

Figure 9. Fraction of frozen pixels in the mTC region 16 calculated from SMOS F/T (blue line) and FT-ESDR (green line) datasets using data from both AM and PM orbits. A five-day filtering was added to FT-ESDR data. Datasets cover years 2010 – 2016.

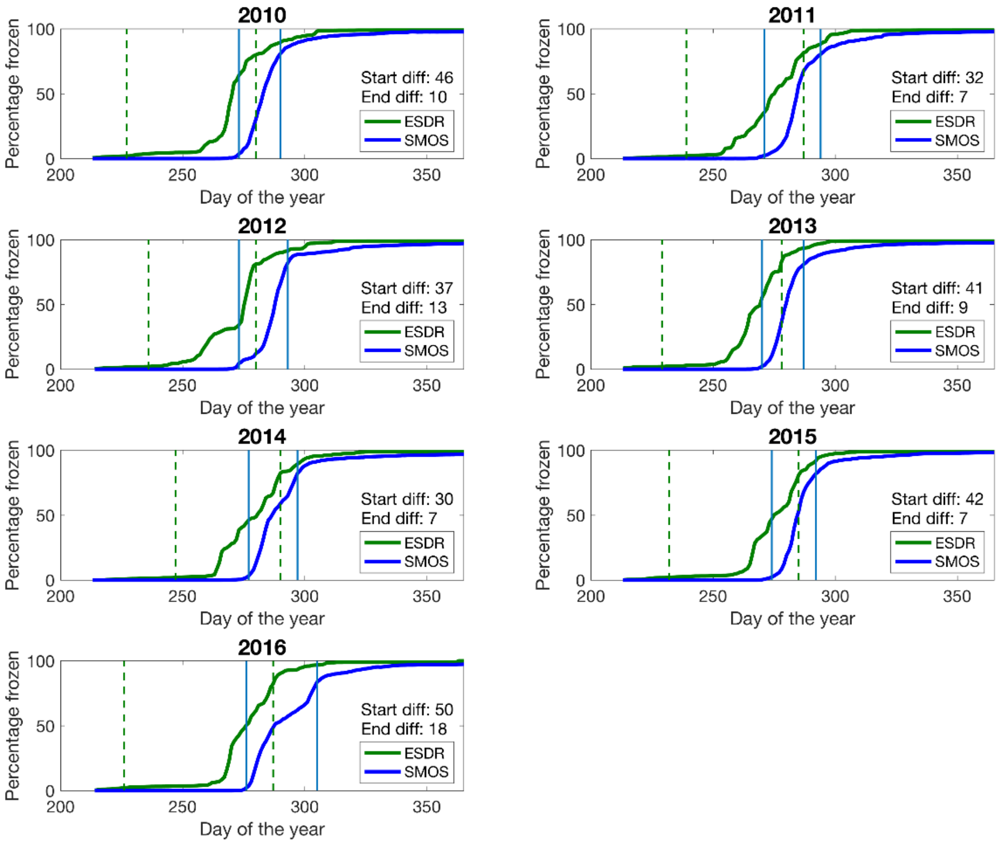

Figure 10. Fraction of frozen pixels in the mTC region 16 calculated from SMOS F/T (blue line) and FT-ESDR (green line) datasets. A five-day filtering was added to FT-ESDR data. For FT-ESDR, only AM orbits are included into analysis. Datasets cover years 2010 – 2016.

Table 3. Difference for the start and the end of the soil freezing between the SMOS F/T and FT-ESDR datasets for mTC regions 1 – 4, 15, 16, 23 and 29. The thresholds of the percent of frozen pixels for the starting date and end date were set to 2% and 80%, respectively. The difference is given in days; positive value: FT-ESDR estimates the freezing earlier, negative value: SMOS F/T estimates the freezing earlier.

	Start of freezing, difference in days								End of freezing, difference in days							
mTC	**1**	**2**	**3**	**4**	**15**	**16**	**23**	**29**	**1**	**2**	**3**	**4**	**15**	**16**	**23**	**29**
2010	12	47	12	15	3	8	74	4	-1	24	9	30	5	10	72	17
2011	10	42	12	1	10	6	36	4	7	20	5	24	13	7	4	3
2012	29	51	4	17	6	12	38	3	7	12	25	19	12	13	4	-9
2013	3	22	5	14	5	10	4	10	12	16	4	5	8	9	34	20
2014	5	37	9	36	4	12	16	-4	10	21	13	14	6	7	-5	27
2015	8	43	-3	13	2	6	15	13	11	21	4	14	1	7	16	7
2016	10	31	4	8	5	8	5	2	3	17	18	20	1	18	10	13
Max-Min	26	29	15	35	6	6	70	17	13	12	21	25	12	11	77	36
Mean	11.0	39.0	6.1	14.9	3.6	8.9	26.9	4.6	7.0	18.7	11.1	18.0	6.6	10.1	19.3	11.1
Std	8.5	9.9	5.3	10.8	2.1	2.5	24.8	5.5	4.7	4.0	8.0	8.0	4.8	4.1	26.3	12.0

2.3.3 Development of Methods Using Carbon Tracker with EO Data

2.3.3.1 Implementation of SMOS F/T data into prior biospheric CH_4 fluxes and its application to CTE-CH_4

Soil F/T data from the SMOS satellite was utilised in building the prior estimates for the biospheric fluxes, in order to improve the seasonal cycle of the emissions in the prior. Biospheric CH_4 fluxes after a soil-freezing period were assumed to be small, until when the soil started to thaw in spring. We defined this ”winter period” based on the soil F/T data, and the prior wetland emissions were set to be constant during this period. The winter period and its emissions were defined for each CTE-CH_4 1°x1° grid. The soil F/T data was first re-gridded from 25 km x 25 km resolution to the CTE-CH_4 grid by taking the ratios of frozen cells. We then assumed that winter period started when the ratio exceeded 0.9 and ended when the ratio passed under 0.9 again. The 2010-2014 monthly mean estimates from the LPX-Bern-DYPTOP were calculated for each 1° x 1° grid cell and the smallest value was taken as the winter period flux of the grid cell.

After the implementation, atmospheric CH_4 values estimated from CTE-CH_4 agreed better with the observed values at high northern latitude sites. The bias and RMSE during winter (November-February) were reduced by 2.3 and 10.9 ppb on average, respectively (Figure 11).

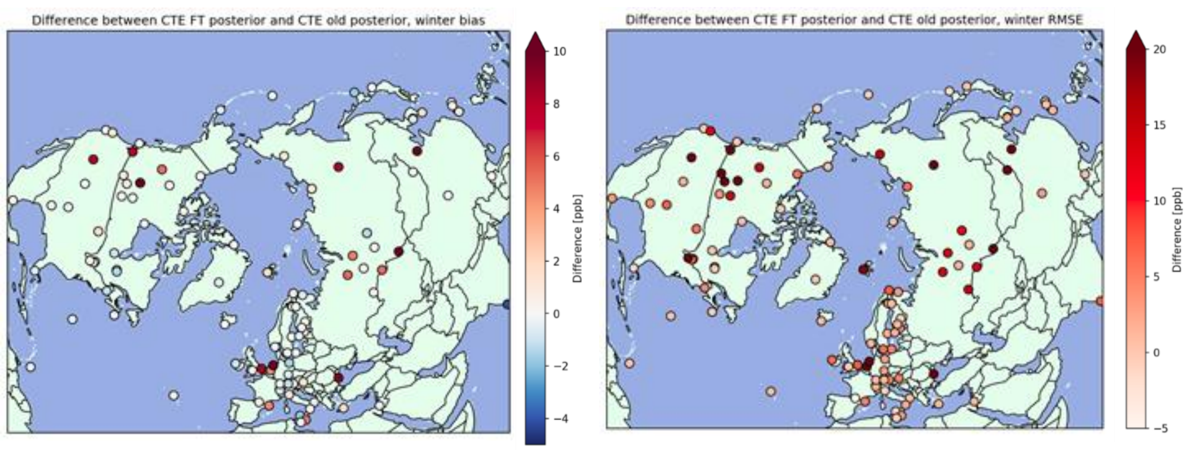

Figure 11. The bias (left) and RMSE (right) differences between posterior SURF1_FT and posterior SURF1 in winter. Positive values denote improvement in agreement with the observations, i.e. decrease in biases and RMSE, and negative values denote worsened agreement.

2.3.3.2 Assimilation of GOSAT and TROPOMI XCH_4 data in CTE-CH_4

CTE-CH_4 was developed to assimilate retrieved XCH_4 data from GOSAT TANSO-FTS (NIES retrieval v2.80) and Sentinel 5P TROPOMI. Atmospheric transport model TM5 (Krol et al., 2005) was first modified to output profiles of atmospheric concentrations and meteorological data. The assimilation scheme was developed then to compare XCH_4 values, taking averaging kernel corrections into account.

In the GOSAT inversion, data correction was applied to account for latitudinal gradient bias. The bias is a common feature among inverse models, such that posterior XCH_4 derived from inversions, assimilating surface observations, tend to be underestimated around the Tropics and Southern Hemisphere. The large-scale differences will be removed before the inversion to assume that atmospheric CH_4 is constrained by the in situ observations to some extent. Five degree zonal mean differences were calculated from the CTE-CH_4 posterior estimates, which assimilated surface in-situ CH_4 observations.

In the TROPOMI inversion, the number of original retrievals is large, and cannot be handled in current CTE-CH_4 setup. Therefore, we reduced the number of data by taking daily averages on 1°x1° grid resolution. CTE-CH_4 originally optimised CH_4 fluxes at weekly resolution, but the number of TROPOMI data was too large to handle in a reasonable computational time even after averaging. We therefore decided to reduce optimisation time window to 3 days, where the number of data are decent to handle computationally, and locations of the data are spread enough to have global coverage.

Hereafter, in the context of inversions and their evaluations, the GOSAT and TROPOMI XCH_4 data are not the original data, but those preprocessed, aggregated and used in the inversions. Those data were assimilated into the system separately and evaluated using the XCH_4 data and surface in-situ CH_4 observations.

On average, about 90 % and 40 % of the GOSAT and TROPOMI data was assimilated at each time step, respectively (Figure 12). The posterior XCH_4 mole fractions show good agreement with the GOSAT and TROPOMI data, where average biases and standard deviation of the differences are 0.5±13 ppb and 5.1±26 ppb, respectively. The agreement was better with the GOSAT data, such that the results from the TROPOMI inversion show overestimations of the posterior XCH_4 values at high latitudes (the SH in winter and the NH in summer) (Figure 12). However, biases in the seasonal cycle of posterior XCH_4 values may be stronger in the GOSAT inversion compared to those in the TROPOMI inversion (Figure 12). The summer NH differences in XCH_4 values may be due to stratospheric biases, or retrieval bias, as the comparison with surface data does not show such strong positive bias (Figure 13).

In the GOSAT inversion, the comparison with in-situ CH_4 observations shows strong latitudinal biases (Figure 14). The agreement in the SH is good (average bias = 1.4 ppb), but strong overestimations are found in the NH (average bias = 37 ppb). This may be due to preprocessing, where latitudinal differences from the in-situ inversions are "over-corrected". Although the agreement at in-situ stations from SURF2 does not show such strong latitudinal biases (Figure 13), the preprocessing of XCH_4 data based on those results may have been too naive. In the TROPOMI inversion, the latitudinal biases in posterior CH_4 values are smaller compared to that in the GOSAT inversion, but underestimation at the NH temperate regions is seen (Figure 14). The agreement with in-situ CH_4 observations show no significant seasonal bias in the posterior CH_4 values from TROPOMI inversion.

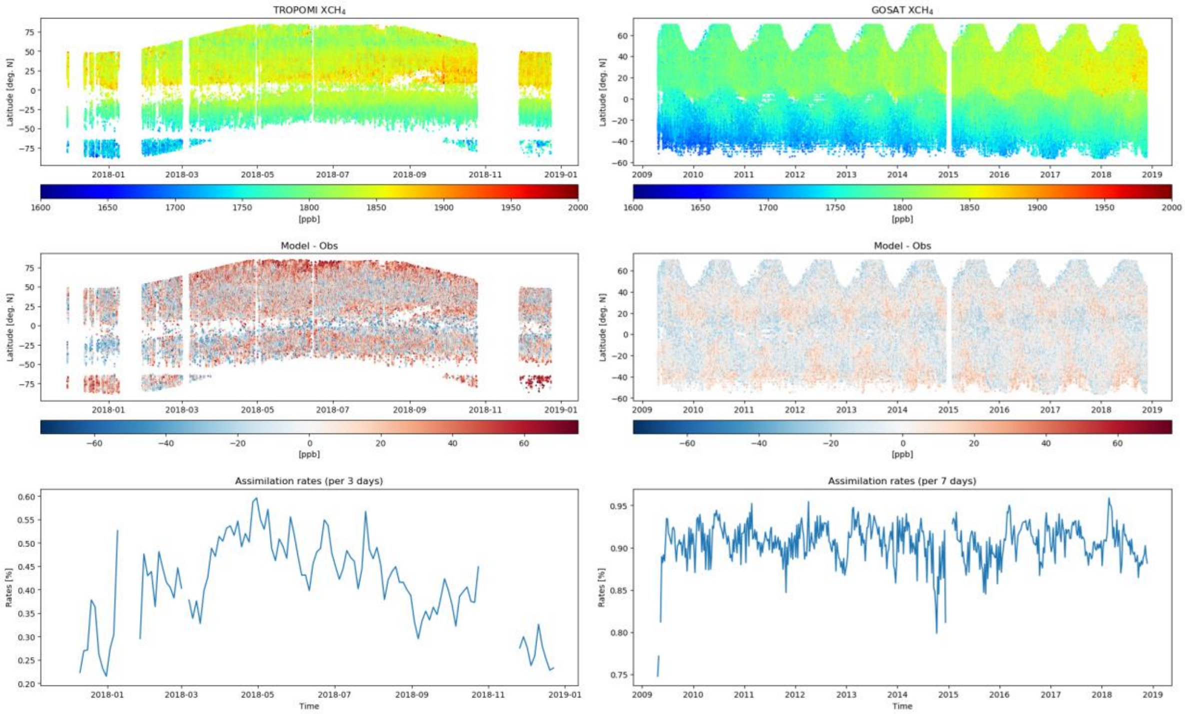

Figure 12. (top) Averaged XCH_4 values from TROPOMI (left) and GOSAT (right) data assimilated in CTE-CH_4. (middle) The differences between the XCH_4 data and the posterior estimates. The bottom panels show assimilation rates per assimilation time window (3-days for TROPOMI and 7-days for GOSAT inversions), where the gaps show days with no data assimilated.

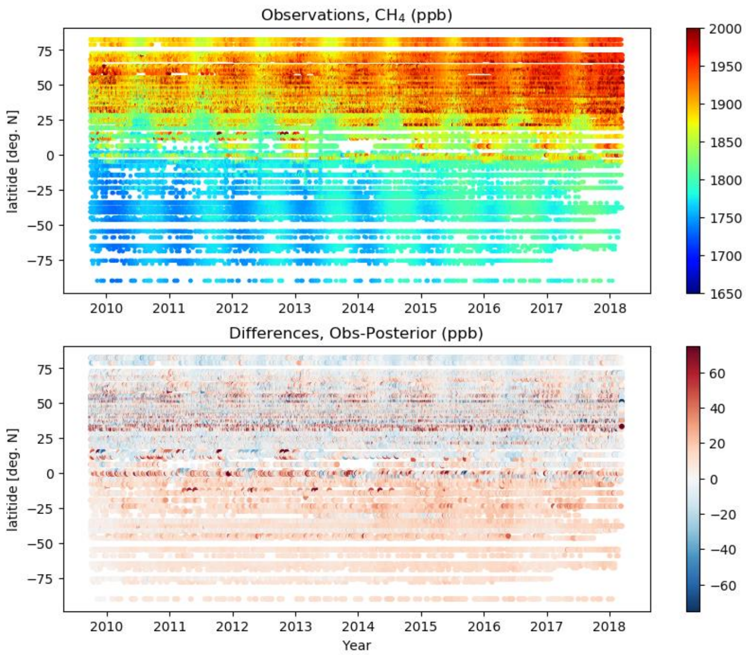

Figure 13. (top) Observed atmospheric CH_4 at surface in-situ stations and (bottom) differences with the posterior atmospheric CH_4 from SURF2. The data show those from assimilated observations.

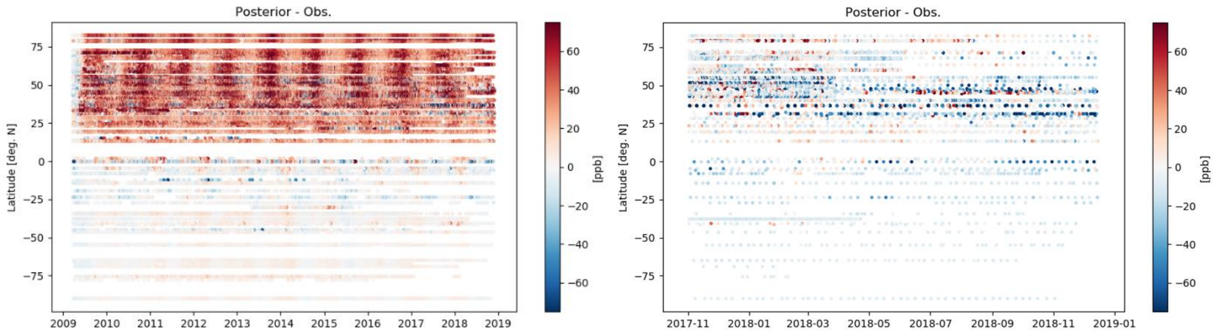

Figure 14. Differences between observed and posterior atmospheric CH_4 from (left) GOSAT and (right) TROPOMI inversion at surface in-situ stations.

2.4 Task 4: Demonstration

2.4.1 Identification of CH_4 Sinks and Sources

The global and northern latitude methane emissions were estimated with inverse model CTE-CH_4 by assimilating in situ concentration observations and satellite column observations in the model, as well as by utilizing the SMOS F/T data for constraining the winter period fluxes in the inversions. Different model set-ups were engaged as presented earlier, namely SURF1, SURF2, SURF1_FT, GOSAT and TROPOMI. SURF refers to inversions assimilating surface atmospheric CH_4 observations and GOSAT and TROPOMI to satellite column observations (Table 4). The main differences in the SURF1 and SURF2 are underlining prior fluxes. SURF1 uses EDGAR v4.2 FT2010 and LPX-Bern DYPTOP (Stocker et al., 2014) for anthropogenic and biospheric sources, respectively, while SURF2 uses those from the latest Global Carbon Project (GCP; Saunois et al., 2019) i.e. extended EDGAR v4.3.2 for anthropogenic and averages from Pouter et al., 2017 for biospheric sources. GOSAT and TROPOMI inversions use priors from SURF2. In all cases, the biospheric and the anthropogenic fluxes were optimized globally. In the following, the emission results from these inversions are presented for northern latitude autumn freezing period, northern high latitude annual emissions and globally, as the changes in the inversion set-ups altered the global fluxes as well as the balances between anthropogenic and biospheric fluxes.

Table 4. Inversions with Carbon Tracker Europe - CH_4 model.

Model set-up	Biospheric prior	Assimilated data	Simulation year(s)
SURF1	LPX-Bern DYPTOP	Surface in-situ	2000 - 2018
SURF1_FT	LPX-Bern DYPTOP + SMOS F/T implemented	Surface in-situ	2010 - 2017
SURF2	Average from Pouter et al., 2017, climatology	Surface in-situ	2000 - 2017
GOSAT	Average from Pouter et al., 2017, climatology	GOSAT XCH_4	2009 - 2018
TROPOMI	Average from Pouter et al., 2017, climatology	TROPOMI XCH_4	2018

2.4.1.1 *Methane emissions during soil freezing period*

In the following, CH_4 emissions during the soil freezing period are presented according to SURF1 and SURF2 inversions, which were not utilising soil freeze/thaw (F/T) data in performing the inversions, but only in the post-processing phase to identify soil freezing periods. The aim here is to first quantify the magnitude of freezing period emissions from independent inversion results and later show the impact of actually utilising soil F/T data in performing the inversions (SURF1_FT) and results from a multi-year inversion utilising satellite CH_4 columns (GOSAT).

The sum of all freezing period days in the northern latitudes and biospheric methane emissions during the freezing period days, as predicted by the inversions, are shown in Figure 15 for the period of 2010 - 2017. The posterior emissions are lower than prior emissions in the surface inversions almost all years (except SURF1 in 2015). The total posterior emissions (anthropogenic + biospheric) are also lower than the prior. In SURF2 the biospheric prior emission was higher than in SURF1 and strongly decreased in the posterior, whereas in the GOSAT inversion the posterior was increased from the prior. However, here the GOSAT inversion results are secondary to in situ inversions because the column data availability is low during the freezing period due to diminishing irradiation. The posterior biospheric emissions of SURF2 are lower than those of SURF1, except in 2014 and 2017. The posterior emissions of SURF1_FT are in between those of SURF1 and SURF2 (Table 5).

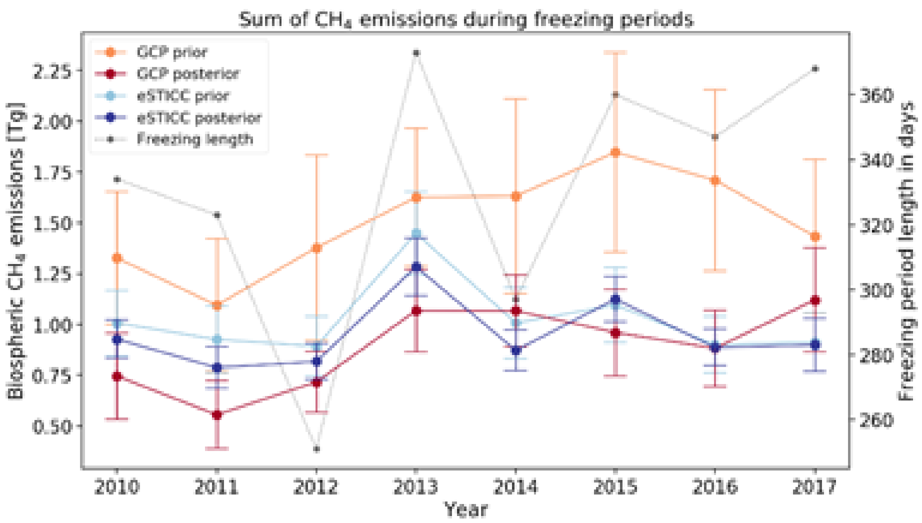

Figure 15. The sum of methane emissions during soil freezing periods and the sum of soil freezing period lengths from eight mTC regions in northern latitudes according to SURF1 (ESTICC) and SURF2 (GCP2018) inversions.

The biospheric emissions during freezing periods vary from 0.55 Tg (SURF2, 2011) to 1.28 Tg (SURF1, 2013, Figure 15, Table 5). On average, according to SURF1, the biospheric emissions during freezing period are 5.4 (4.4 - 7.7)% from the annual biospheric emissions and 3.1 (2.6 - 4.3)% from the annual total emissions. According to SURF1_FT, the biospheric emissions are on average 4.2 % from the annual biospheric emissions. The highest emissions occurred in 2013 in the SURF1 run and 2017 in the SURF2 run. The number of freezing period days was second highest in 2017 after 2013. The two latest years experienced long freezing periods in many regions. Especially in 2016 the mTC region covering Northern Europe (Fennoscandia) did not freeze completely during the winter. However, as the region and its emissions are small in comparison to some other regions like those in Canada including Hudson Bay Lowlands and in Russia including Western Siberian lowlands, the methane emissions from Fennoscandia did not hugely increase the total emissions.

Table 5. Freezing period biospheric CH_4 emissions at northern latitudes (eight modified Transcom regions) as estimated from CTE-CH_4 [Tg CH_4 yr^{-1}]. For SURF, in-situ atmospheric CH_4 observations are assimilated, for SURF1_FT, the F/T data are used in model implementation, and for GOSAT, the satellite XCH_4 data are assimilated. The averages are calculated from 2010-2017, and min and max refer to minimum and maximum of the yearly freezing period sums.

	Prior mean	Prior min	Prior max	Posterior mean	Posterior min	Posterior max
SURF1	1.02±0.41	0.89±0.13	1.45±0.16	0.95±0.33	0.79±0.10	1.28±0.13
SURF2	1.51±0.64	1.09±0.20	1.85±0.25	0.89±0.44	0.55±0.14	1.12±0.18
SURF1_FT	0.93	0.81	1.32	0.86	0.69	1.21
GOSAT	1.79	1.09	2.72	2.03	1.24	3.02

2.4.1.2 GOSAT and TROPOMI inversions

Inversions assimilating GOSAT and TROPOMI XCH_4 data were performed separately and compared with the inversion results assimilating in-situ atmospheric CH_4 observations (SURF1 and SURF2) (see also Table 4 for inversion setups).

The results show the global annual CH_4 emissions to be 526-561 Tg CH_4 yr^{-1}, and the inversions agree well within the uncertainty ranges (Table 6). However, the satellite inversions tend to result in higher global total emissions than those from SURF. Inversions SURF1, GOSAT and TROPOMI suggests that the prior anthropogenic emissions may be overestimated, while the prior biospheric fluxes from SURF2 may be underestimated, although the estimates are within the uncertainty ranges (Table 6). However, the source separations in SURF2 differ much from the others; although global total is similar to others, the biospheric estimates are much lower, and the posterior anthropogenic estimates are higher than the prior.

The satellite inversions clearly give higher global total posterior biospheric estimates compared to the SURF inversions (Table 6). However, for northern Europe and northeast Russia, the TROPMI inversion shows lower estimates than SURF2, and the differences between the GOSAT and SURF2 inversions are small (Figure 16). For mTC 4, where Canadian Hudson Bay Lowlands are located, the prior from SURF1, the posterior from SURF2 and the posterior from the TROPOMI inversions ranged between 3.2 to 5.6 Tg CH_4 yr^{-1}. The estimates agree well with the previous studies, which range between 2.3 to 5.5 Tg CH_4 yr^{-1} (Peltola et al., 2019). However, the prior from SURF2 and the posterior from the GOSAT inversions are approximately three times higher (13.5 and 14.5 Tg CH_4 yr^{-1}, respectively). Considering together with the evaluation against in-situ surface CH_4 network (Figure 14), we suspect that the prior from the SURF2 and the posterior from the GOSAT inversion overestimate the biospheric emissions in this region. For mTC 15, where Western Siberian Lowland are located, the estimates range between 5.3 to 11.1 Tg CH_4 yr^{-1}, where the estimates from the GOSAT inversion are the highest, followed by the TROPOMI inversion. The estimates are slightly higher than those collected and estimated by Peltola et al. (2019), but within the uncertainty ranges (approx. 3 Tg CH_4 yr^{-1} for SURF2 prior).

The estimated monthly total emissions show that the seasonal cycles for northern Europe is dominated by the biospheric sources. Summer maximum occurs between July to September, and the maximum average monthly total biospheric emissions vary between 0.15-0.38 Tg CH_4 month^{-1} (Figure 17). As is also seen from Figure 16, the posterior estimates from the TROPOMI inversion are much lower than those from other inversions. In addition, little variation is found in the TROPOMI inversion during June-August estimates, i.e. reaching to near summer-maximum values earlier than the other inversions (Figure 17). We suspect that this may be partly due to seasonal bias in the TROPOMI XCH_4 retrievals (Figure 3), but further analysis is needed.

The uncertainty estimates in TROPOMI inversion was significantly smaller than the other inversions, indicating strong forcing due to the large number of assimilated data. Note however, that smaller uncertainty does not necessarily mean better estimates.

Table 6. Global annual CH_4 emissions estimated from CTE-CH_4 [Tg CH_4 yr^{-1}]. For SURF, in-situ atmospheric CH_4 observations are assimilated, and for GOSAT and TROPOMI, the satellites' XCH_4 data are assimilated. For SURF1 and SURF2, the averages are calculated from 2000-2017, while for GOSAT and TROPOMI, the averages are calculated only from 2018. The totals are the sum of fluxes from the biospheric and anthropogenic sources, fires, termites and oceans. The uncertainty ranges are standard deviations of 500 members used in the ensemble Kalman filter.

	Total prior	Total posterior	Anthropogenic prior	Anthropogenic posterior	Biospheric prior	Biospheric posterior
SURF1	541±80	532±72	346±52	339±50	152±61	149±51
SURF2	523±77	526±68	318±67	334±63	139±36	126±27
GOSAT	555±86	561±81	349±77	341±75	142±38	156±32
TROPOMI	555±86	550±65	349±77	325±63	142±37	162±18

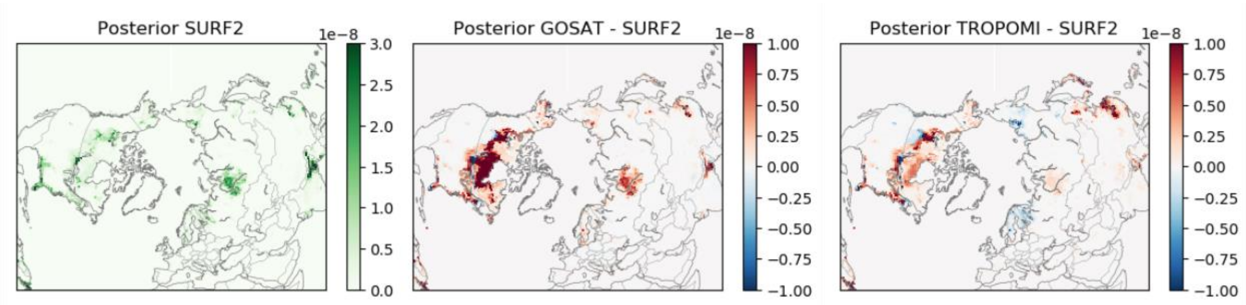

Figure 16. Average biospheric CH_4 fluxes over northern latitudes estimated from CTE-CH_4, and their differences between inversions [mol m^2 sec^{-1}].

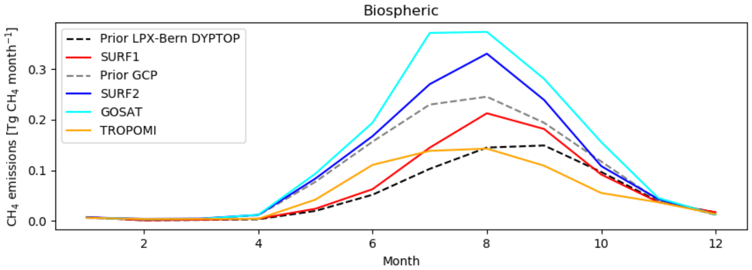

Figure 17. Average monthly CH_4 emissions over Europe, >60°N, estimated from CTE-CH_4 for biospheric sources. For TROPOMI, the estimates are from 2018, and the others are mean over 2017-2018.

2.4.1.3 Inversion with SMOS F/T data implementation

The biospheric a priori with SMOS F/T data implementation (see Section 2.3.3.1 for implementation of SMOS F/T data into the prior biospheric CH_4 fluxes and its application to CTE-CH_4) was used in CTE-CH_4 with a set-up similar to SURF1. Implementing the SMOS F/T data to a biospheric a priori reduced the biospheric methane emissions approximately 0.41 Tg per year. After the optimization with CTE-CH_4, the magnitude of the decrease remained the same when compared to the optimized result without the SMOS F/T data implementation. The decrease was the most prominent in Central Russia (mTC 15) which was responsible for 48 % of the total decrease. Also, Hudson Bay Lowlands, Alaska and Northern Fennoscandia, regions with large wetlands, were affected noticeably (see Figure 18). The average annual total, anthropogenic and biospheric emission estimates of SURF1, SURF1_FT and SURF2 in the northern mTC areas are shown in Table 7. The anthropogenic emissions increased in the northern latitudes which was mostly due to the increase in Central Russia, partly compensating the decrease in biospheric emissions.

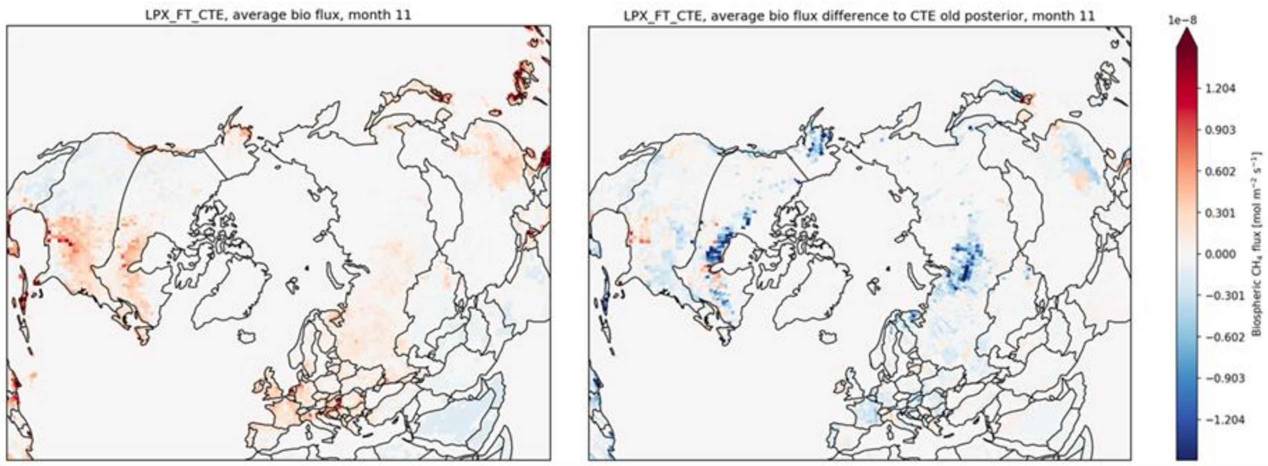

Figure 18. Left: The average biospheric flux estimation of posterior SURF1_FT in November. Right: The difference of the average biospheric fluxes in November between posterior SURF1_FT and posterior SURF1.

Table 7. Annual CH4 emissions estimated with CTE-CH4 [Tg CH4 yr-1] from northern mTC areas. SURF1 is optimized with the original LPX and SURF1_FT with the FT data implemented in LPX. The averages are calculated from 2010-2017. The totals are the sum of fluxes from the biospheric and anthropogenic sources, fires, termites and oceans.

	Total prior	**Total posterior**	**Anthropogenic prior**	**Anthropogenic posterior**	**Biospheric prior**	**Biospheric posterior**
SURF1	37.25	40.64	16.26	16.49	17.49	20.37
SURF1_FT	36.97	40.51	16.26	16.71	17.12	20.02
SURF2	54.13	40.78	13.73	15.29	35.92	20.59

2.4.2 Trend Analysis

2.4.2.1 EO based freeze and thaw data

Trend analysis using EO data were performed over mTC regions 15 and 16 (see Figure 5) concentrating on the soil freezing period. To determine the freezing period of a mTC region, the daily ratio of frozen pixels to total area was calculated for FT-ESDR and SMOS data separately. For both datasets, the area was limited to only pixels where less than 10% of the dates were missing data in the SMOS product during the freezing periods (August – February) of the years 2010 – 2016 combined. The start of the freezing was determined when 2% of the area was frozen, and the end when 80% was frozen.

The freezing periods acquired from FT-ESDR data were compared to those from SMOS data for years 2010 – 2016, and the mean of the differences in both the start and end days were calculated. The FT-ESDR dataset was then shifted using this mean difference – a simple bias correction based on results obtained from WP 320 (see Section 2.3.2). The bias corrected ESDR is here referred as scaled ESDR.

The trend analysis results are shown in Figure 19 and Figure 20 for mTC regions 15 and 16, respectively. Top panel shows the estimated start and end dates for the freezing period, bottom panel shows the length of the freezing period. The estimates are given for scaled ESDR data and for SMOS F/T data. SMOS F/T data extend the FT-ESDR by three freezing periods. The scaled ESDR and SMOS F/T results are very consistent.

For both regions, the start of freezing has a clear trend towards later days. For mTC region 15: 0.33 days/year (p-value of 0.0045) and region 16: 0.38 days/year (p-value of $6e^{-6}$). For the end of freezing, no significant trends were found. This has led to shorter freezing periods, 0.44 days/year (p-value 0.00092) and 0.4 days/year (p-value 0.000012) for regions 15 and 16, respectively.

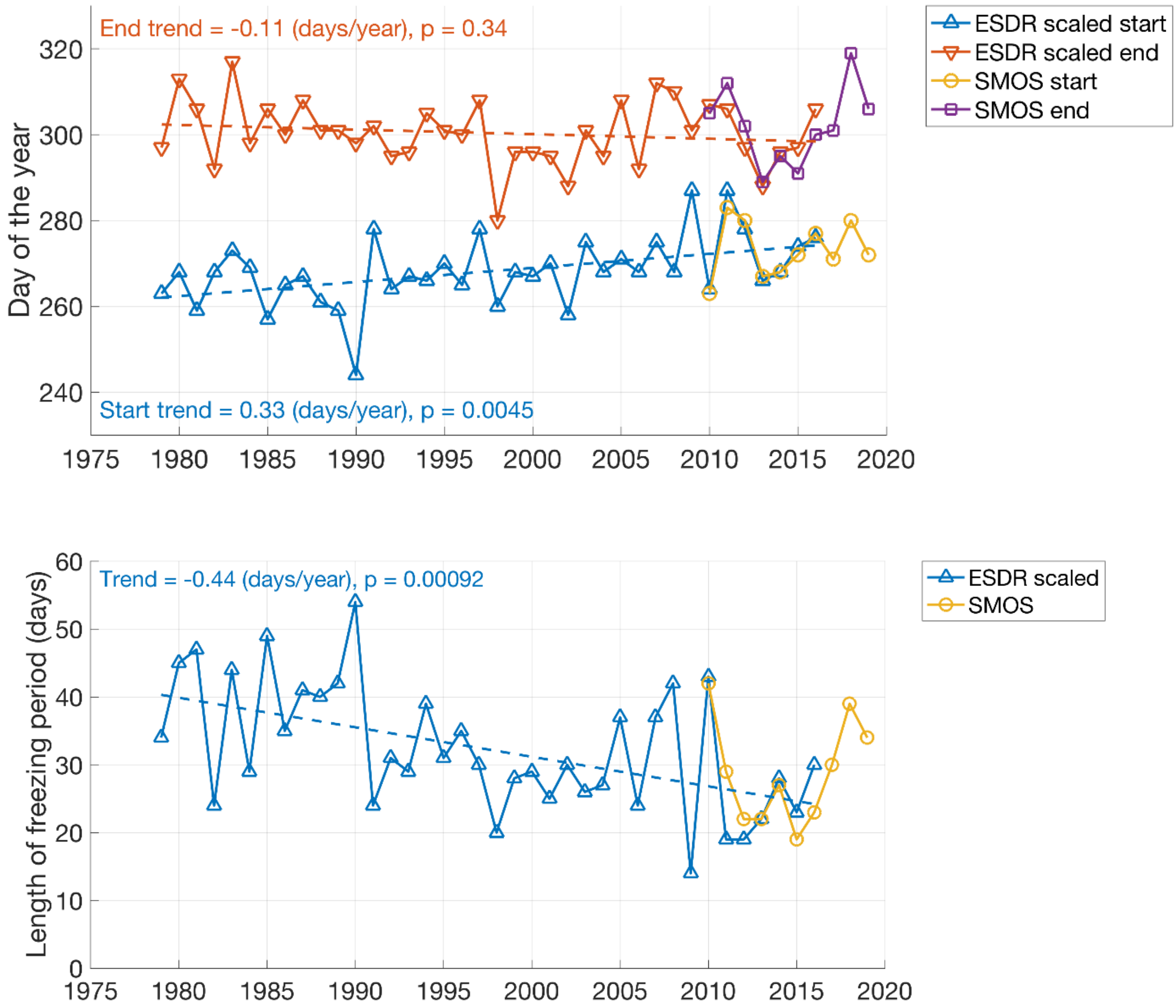

Figure 19. Top: The soil freezing period start and end dates and their trends for autumns 1979-2016 estimated from combined SMOS F/T and FT-ESDR dataset for mTC region 15. For years 2010-2019, included also estimated dates based only on SMOS F/T data. Bottom: Length of the freezing period in days for mTC 15

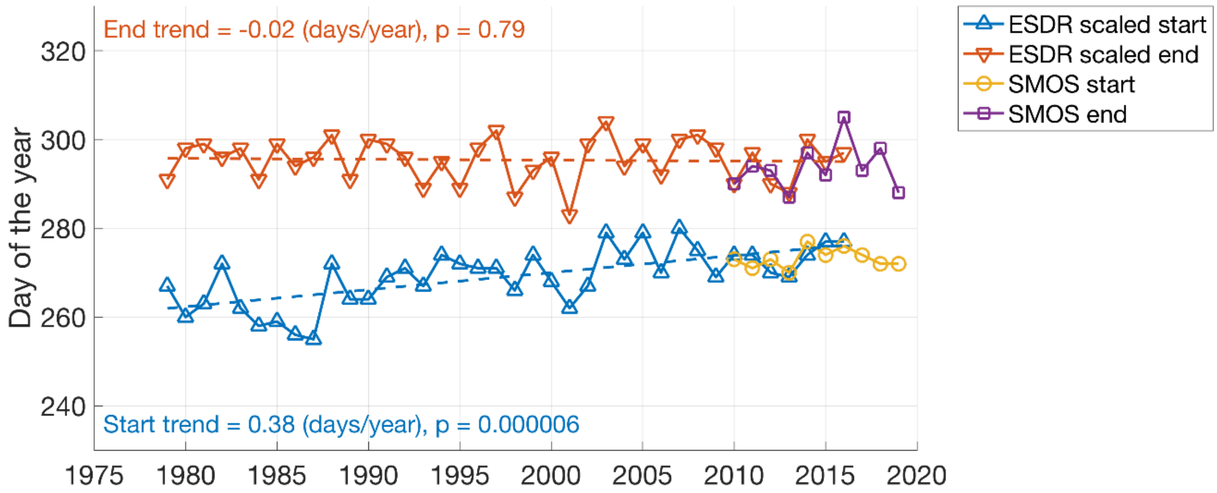

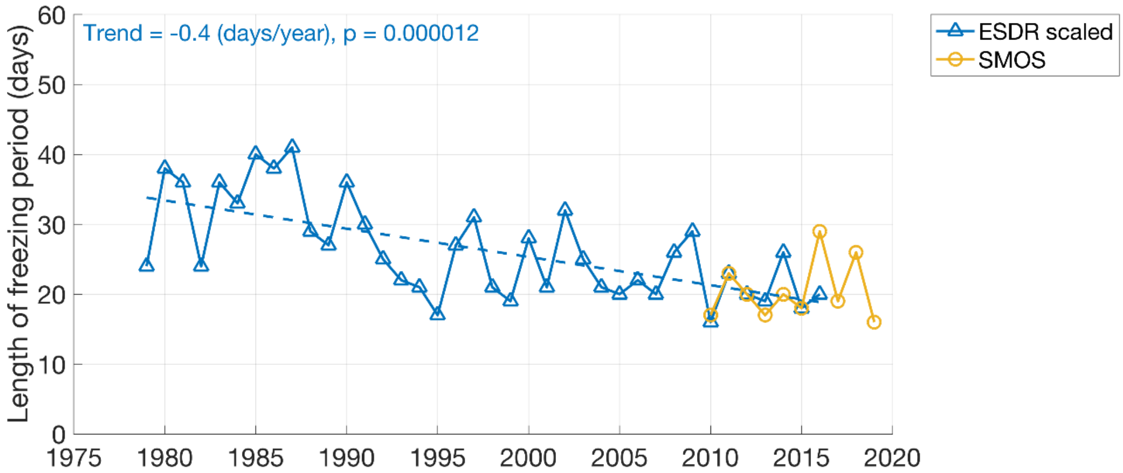

Figure 20. Top: The soil freezing period start and end dates and their trends for autumns 1979-2016 estimated from combined SMOS F/T and FT-ESDR dataset for mTC region 16. For years 2010-2019, included also estimated dates based only on SMOS F/T data. Bottom: Length of the freezing period in days for mTC 16

2.4.2.2 Global total CH_4 emissions from CTE-CH_4 inversions

The estimated average trend over 2000-2018 from CTE-CH_4 inversions show an increase in global total emissions of approximately 3.1 (1.8 - 4.5) Tg CH_4 yr^{-2}, which is mostly associated with the increase in anthropogenic emissions (2.7 - 5.5 Tg CH_4 yr^{-2}). The trends in global total biospheric emissions are unclear; the posterior estimates from SURF inversions and prior from LPX-Bern DYPTOP show negative trends (-0.5 to -1 Tg CH_4 yr^{-2}), while posterior estimates from the GOSAT inversion show slightly positive trends (0.6 Tg CH_4 yr^{-2}).

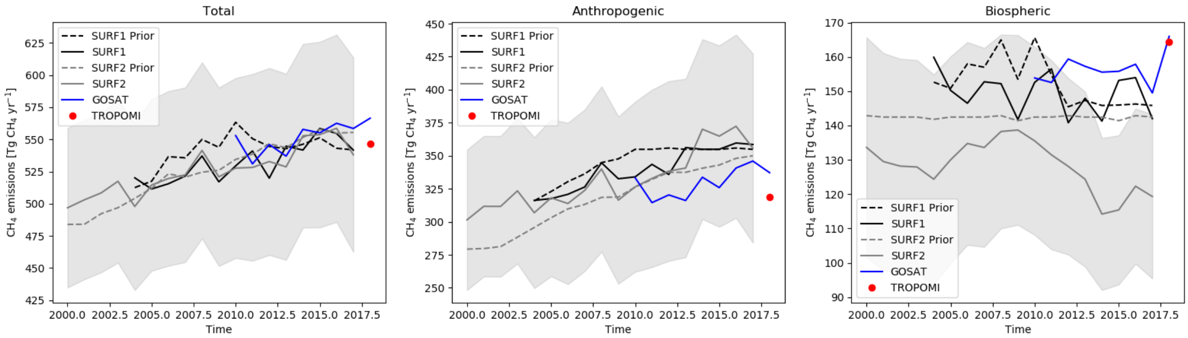

Figure 21. Global annual posterior CH_4 emission estimates from CTE-CH_4. The grey shaded area illustrates the uncertainty range from SURF2.

2.4.2.3 Soil freezing period emissions in northern Siberia

The extended soil freeze/thaw data were used to define the biospheric freezing period emissions in regions mTC 15 and mTC 16 (northern Siberia). The emission estimates from CTE-CH_4 run SURF1 were used.

The freezing period emissions in mTC 15 are shown in Figure 22. SURF1 shows decreasing trends with 3-5 Gg less methane per year for mTC 15. The start date of the freezing period delayed by 0.33 days per year, and it is probably causing the reduction of the biospheric methane emissions. The largest emissions appear in the beginning of the freezing period (Development and Evaluation Report WP310), and thus the freezing period emissions depend on the start date of the freezing period. The posterior trend is larger than the prior trend. Also, only posterior trend is significant ($p < 0.05$). The freezing period emission estimates of SURF1 in the region mTC 16 are shown in Figure 22. The emission estimates of SURF1 show an increasing trend, which is not significant.

The length together with the start date of the freezing period impacts the freezing period emissions, and high emissions seem to be linked to earlier start dates. To have more robust method to study the emissions, the same period of every year was selected from CTE-CH_4 runs, taken as the period between earliest start date (mTC 15: DOY 258 and mTC 16: DOY 262) and the latest end date (mTC 15: DOY 312 and mTC 16: DOY 304) defined with the FT-ESDR dataset starting from the year 2000. The trend analysis did not reveal significant emission trends for this fixed period. The fixed period emissions need to be examined in more detail including the role of soil temperature determining the pre-freezing period emissions. The existence of a significant emission trend during soil freezing period or fixed autumn period remains somewhat inconclusive in light of the current results.

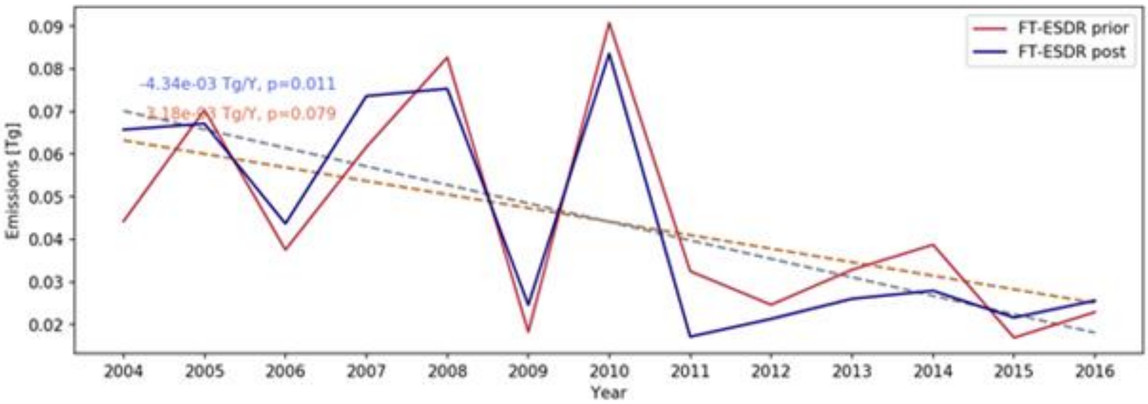

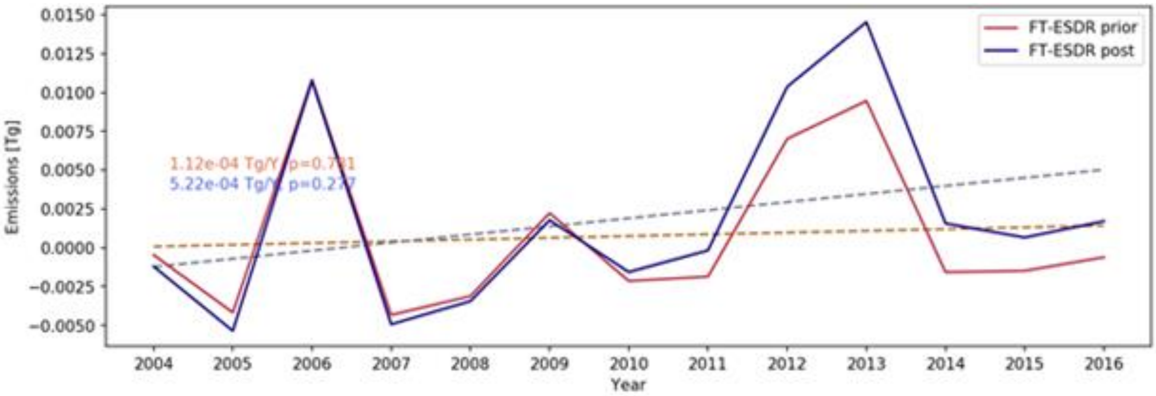

Figure 22. Biospheric freezing period emission estimates of SURF1 in mTC 15 (top) and 16 (bottom). Prior emissions are with red solid line and posterior emissions with blue solid line. The trends of prior and posterior emissions are shown with dashed lines.

2.4.2.4 Methane concentration trend estimates in northern Siberia

The CH_4 concentration trends from CTE-CH_4 were estimated in every atmospheric layer for both surface and GOSAT data assimilations at the mTC regions 15 and 16. The growth rates in each layer were quantified using the Dynamic Linear Model (DLM) which allows the consideration of nonlinearity in the trend, in addition to a varying seasonal cycle. The analysis method also results in robust error estimates for the growth rate. The DLM has recently been applied in CH_4 time series modelling for both ground-based and satellite-based measurements (Kivimäki et al., 2019; Karppinen et al., 2020). The DLM trend estimates for CTE-CH_4 were evaluated at Sodankylä, Northern Finland, against the ground-based FTS-retrieved and ACE-FTS satellite-retrieved growth rates (Karppinen et al., 2020), and generally a good agreement was found (for details, see Demonstration report).

The CTE-CH_4 model concentration trends at the modified TransCom regions 15 and 16 are shown in Figs. 22 and 23, respectively. Because the project focus is on studying the surface fluxes and resulting atmospheric concentrations, the time series for the CTE-CH_4 layer closest to the surface at both regions are shown in Fig. 24 for both surface and GOSAT inversions.

In the mTC 15 region, the CTE-CH_4 results using surface or satellite data in the assimilation agree to a large extent on the CH_4 growth rates during 2010–2018 both in the troposphere and at higher altitudes. In the surface data inversion, the concentrations closest to the surface have been increasing throughout the 18-year time series (see Fig. 24). In the upper boundary layer and the free troposphere, the concentration trends flattened in 2004–2006, which was seen as a minor delayed effect also in the stratosphere few years later. The tropospheric concentration growth rate has peaked in early 2002–2003, again in 2007–2008 and latest in 2014–2015. The latter is also clearly seen in the GOSAT inversion results. Both model results suggest a recent slowdown in the surface and tropospheric trends but agree on a strengthening increase at 10–15 km altitude range, which could be a lag effect of the 2014–2015 peak growth in the troposphere. In the upper atmosphere, the results for GOSAT and surface inversion differ for the latest years. The GOSAT inversion suggests a notable negative trend in the upper atmosphere, strongly contrasting the positive tropospheric – lower stratospheric trend, while the surface inversion does not show such a systematic trend throughout the upper atmospheric layers. The alternation between positive and negative trends seems to be characteristic of the upper atmosphere CH_4 concentration (see Karppinen et al., 2020), and may reflect changes in the atmospheric OH sink or transport patterns from lower latitudes.

In the mTC 16 region, the CTE-CH_4 results using surface or satellite data in the assimilation agree to a large extent on the CH_4 growth rates during 2010–2018 both in the troposphere and at higher altitudes, as was seen also for the mTC 15 region. A significant difference appears to be the contrast between the troposphere and the upper atmosphere growth rates, which is more pronounced for GOSAT inversion, especially in the latest years. The tropospheric concentration growth rate has peaked in early 2002–2003, again in 2007–2008, also somewhat in 2011–2012 and latest in 2014–2016. These results are mostly similar to what we found for mTC 15; however, this is not unexpected since the concentration analysis is always affected by atmospheric transport, in addition to local fluxes. The two latter periods of increasing concentrations are also seen in the GOSAT inversion results. A potentially interesting difference is that the surface inversion suggests a recent slowdown in the surface and tropospheric trends, yet the satellite inversion estimates a persisting positive trend. However, the DLM results loose accuracy towards the edges of the time series, which is reflected in the increased error estimates for the trend towards the edges (see Fig. 24).

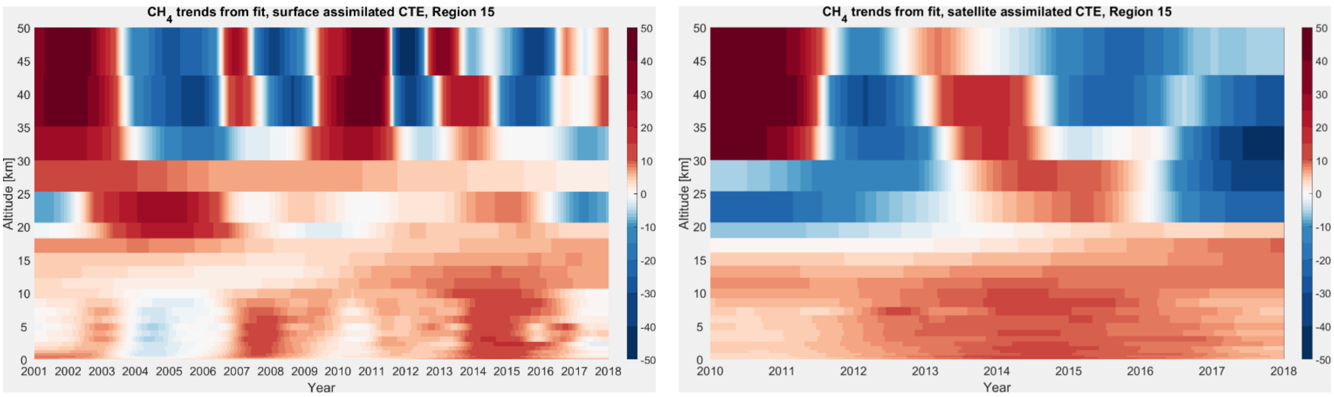

Figure 23. Methane concentration growth rate in different atmospheric layers in mTC 15. Blue colors indicate a decreasing trend in the concentration, red colors refer to an increasing atmospheric growth rate. Left panel: CTE-CH_4 inversion based on in-situ data for 2001–2018; right panel: CTE-CH_4 inversion based on GOSAT data for 2010–2018.

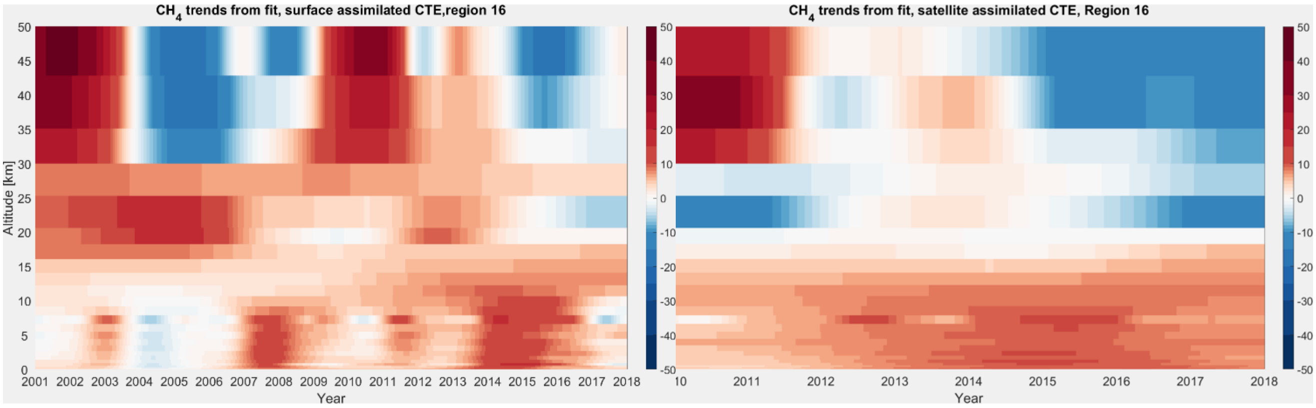

Figure 24. Methane concentration growth rate in different atmospheric layers in mTC 16. Blue colors indicate a decreasing trend in the concentration, red colors refer to an increasing atmospheric growth rate. Left panel: CTE-CH_4 inversion based on in-situ data for 2001–2018; right panel: CTE-CH_4 inversion based on GOSAT data for 2010–2018.

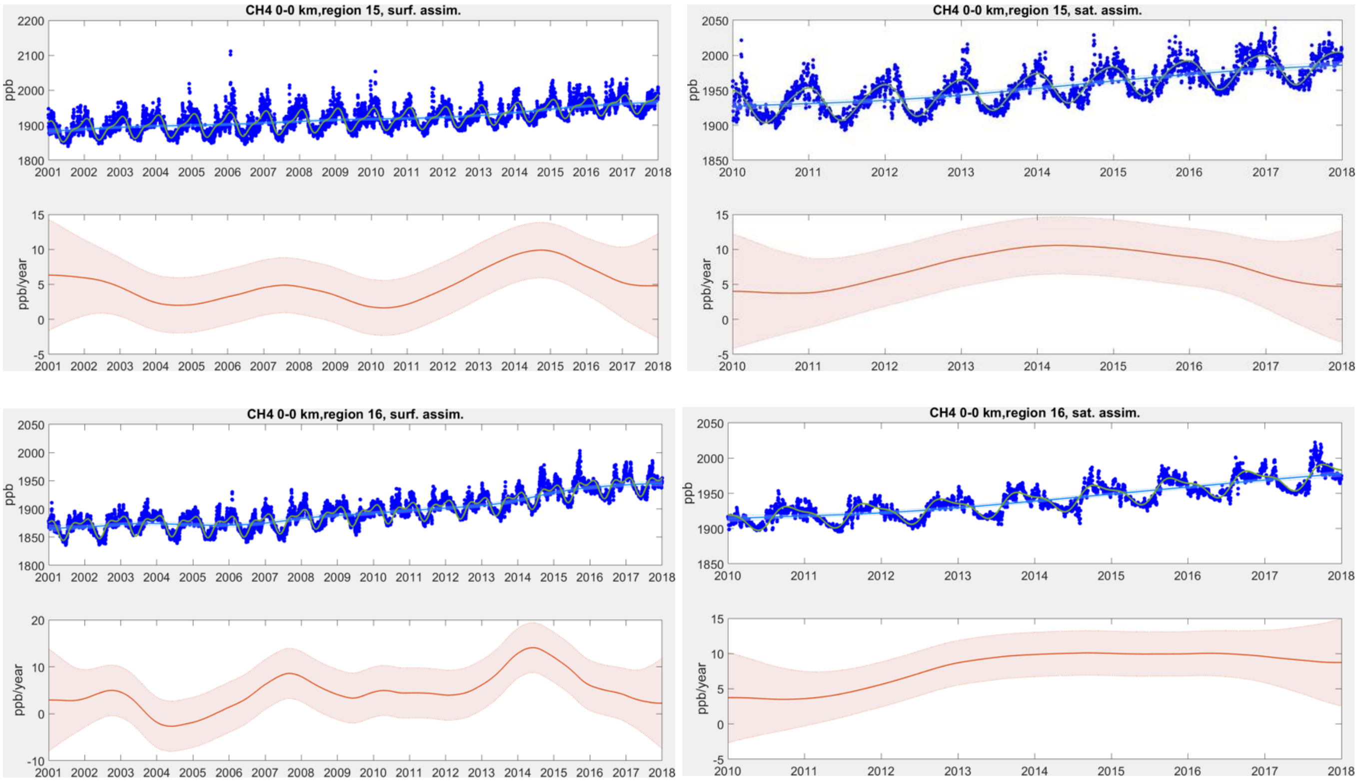

Figure 25. Time series of CTE-CH_4 concentration in the lowest level of the troposphere (e.g., closest to the surface). Upper left: Surface inversion for mTC 15 region; Upper right: GOSAT inversion for mTC 15 region; Lower left: Surface inversion for mTC 16 region; Lower right: GOSAT inversion for mTC 16 region.

3 Impact Assessment and Scientific Roadmap

Here we summarize the project findings and impacts and provide important information for the future studies on how to further continue this work. We have divided this section to scientific and methodological developments, and a roadmap.

Impacts of the project are summarized as follows. The project showed the potential of innovatively using versatile data sources together: satellite soil FT data, atmospheric column data, in situ flux and concentration data were used together with atmospheric inverse modelling in assessing the northern latitude methane emissions. Implementation of soil FT data improved inverse modelling results, and assimilation of satellite column concentrations manifold the amount of informative data used for flux estimations. Experience was gained in using satellite big data in inversions, useful for future satellite missions. Residual biases in satellite retrievals were noted to have a significant impact on the inversion results and complicate the interpretation of emissions. The project contributed to improved understanding of the northern latitude methane emissions, and methane emissions during soil freezing period. Understanding of methane dynamics in the upper layers of the atmosphere was improved, as well as changes in soil freezing period length over the recent decades.

3.1 Scientific developments

3.1.1 Methane emission production processes during soil freezing period

In this study, we found that methane emissions during the soil freezing period are non-zero and are correlated with soil freezing period length. However, we did not find clear evidence towards the lengthening of the emission period over the years. The start date of the soil freezing periods shifted later in northern Siberia but the end date, or complete freezing, did not change, resulting in shortening of the soil freezing period. Overall, we found both increasing and decreasing trends in methane emissions during freezing periods and during autumn (mid-September to early November). These trends deserve more thorough examination for all regions using various data analysis methods and models, including atmospheric inversion, process-based models and carbon cycle data assimilation systems (CCDAS) which combine the two previous (Rayner et al., 2005).

3.1.2 Seasonal cycle of the Arctic biospheric methane emissions

This project focused on late autumn – winter season, and soil freeze/thaw status. The estimation of the methane emissions from the full winter period, when the soil is frozen, was improved through combining the SMOS soil F/T information with prior fluxes in inversions. In addition to being constrained by timing of soil thaw in spring, the northern high latitude methane emissions are sensitive to wintertime meteorological and land surface conditions, such as the amount of rainfall in form of water or snow and accumulation and structure of snow cover. Satellite data related to precipitation, snow water equivalent, inundation extent and soil moisture is available from e.g. Copernicus and should be utilised in further analysis of the cold period methane emissions together with GHG column observations and modelling. Here new advances in land surface process modelling might also give insights into the connections between evolution of snow cover, respiration and methane formation in soil and diffusion through snowpack during winter. In situ data related to GHGs, soil and snow is of pivotal importance, and e.g. drone measurements of atmospheric composition and surface variables provide new possibilities for regional upscaling to meet satellite and model resolutions.

3.1.3 Focus on permafrost

The investigations and trend analysis carried out in this project should be repeated for different region definitions. The modified TransCom regions 15 and 16 considered in this project include both permafrost and non-permafrost terrain. In order to better characterise these and the trends of interest for the active season, the permafrost and non-permafrost regions could be further clustered based on the active layer type. In addition to repeating the trend analyses for these regions, additional satellite and meteorological reanalysis data should be considered.

3.1.4 Using multiple GHG satellites in atmospheric inversions

In this project, methane column data from two satellites, GOSAT and Sentinel 5P/TROPOMI, was assimilated to the CTE-CH_4 inversion model with promising results. GHG satellite missions are expected to increase in near future, and GHG data from various satellites will become available (Crisp et al., 2018) for validation and assimilation in atmospheric inversions. Particularly interesting are GOSAT-2, MERLIN, and the planned Copernicus Anthropogenic CO_2 Monitoring Mission. Also, GHG retrievals using the infrared radiation (e.g., from IASI) remain underused in methane inverse modelling and could be particularly useful in the high latitudes, considering the polar night. However, these satellites provide data of different quantities as e.g. their measurement techniques (e.g. pointing scanning in GOSAT vs pushbroom scanning in Sentinel 5P), swath width, footprint resolutions, and data quality are different. The differences found for GOSAT and TROPOMI inversion results in this project gave an example on the implications for inverse modelling. Therefore, more detailed and advanced data assimilation schemes will be required to take those differences into account in atmospheric inverse modelling. In addition, using in situ data together with satellite data is often necessary and creates an additional level of complexity in configuring the data assimilation set up. Adding other remotely observable tracers like e.g. carbon monoxide to inversion set-up potentially provides more information about the origin of emissions, but also creates new challenges for simulations and interpretation of results.

3.1.5 Partial column retrievals

Combining information from various satellites and other measurement techniques (e.g. AirCore and aircrafts) helps us to understand vertical profiles of the GHG concentrations. Partial column data would be useful to study the lower and upper atmosphere separately. Using information from lower atmosphere, we would be able to better detect local and instantaneous emission signals. Due to abrupt thawing of ice, methane emission burst may occur from craters in the permafrost regions and ice cracks in the Arctic sea and lakes. In addition, local anthropocentric emissions from oil and gas plants, and leakages from, e.g., oil and gas industry needs to be better distinguished.

The partial column information would also be useful for developing transport models. From the comparison with AirCore measurements, and trend analysis on vertical profiles, we found that the methane depletion and trends in the stratosphere is not yet well resolved in the model. Partial column data can be used as validation tools for such model development.

3.1.6 Identification of anthropogenic sources

This project focused on the NHL biospheric methane emissions. However, the emissions from anthropogenic activities are also high, exceeding biospheric emissions at latitudes 50°N - 90°N. There are approximately 477 million people living in latitudes north of 50°N (GPWv4; Doxsey-Whitfield et al., 2015), and the regional oil and gas industry is strong and evolving. The regional anthropogenic methane emissions are also considered to be sensitive to climate change, such that expansion of sea routes, oil and gas industries and agriculture can be expected due to warming. The seasonal cycle of anthropogenic emissions may also change; heating is a large source of GHG emissions during winter currently, which may reduce due to warming, and more energy may be needed for summer cooling in the future. In order to better understand the current situation and future changes, we need to examine NHL anthropogenic emissions more closely using various socio-economic and industry-related data. Current satellite observations (such as Sentinel 5P) and upcoming active instruments (such as MERLIN) provide novel opportunities to detect emission sources in high resolution up to the level of individual industrial complexes.

3.1.7 Validation datasets

In this project, we used measurements such as in-situ methane flux and concentration measurements, TCCON, and AirCore data for model validation, focusing on a region with extensive data coverage. The number of validation datasets is increasing throughout the NHL, and we should continue to make use of them. Currently, most of those measurements are located on remote sites, based on the tradition to quantify emissions from natural sources. The number of measurement sites and studies in agricultural lands are increasing, but further development on measurement techniques and number of locations will be needed to better understand emissions from e.g. oil and gas plants, leakages, livestock farms and landfills. A particularly interesting development is the emerging Collaborative Carbon Column Observing Network (CoCCON; Frey et al., 2019) of portable EM27/SUN spectrometers that are expected to make GHG satellite validation increasingly versatile, especially with the inclusion of anthropogenic emission environments. For example, FMI will host an EM27/SUN in Helsinki to contribute to urban high-latitude satellite validation. Cooperation with private companies can also possibly provide more opportunities for such developments, especially for the validation of anthropogenic emissions.

3.1.8 Dedicated Arctic campaigns

To advance our understanding of the information brought by multiple satellites measuring soil, atmospheric composition, precipitation, and other variables that provide data on the Arctic methane emissions and its linkages to soil, dedicated campaigns would be in a key role. Several relevant measurements that are necessary for upscaling from in situ to satellite-scale (such as drone and balloon-borne AirCore measurements), are work-intensive and therefore their best benefits are obtained in a systematic and coordinated effort in conjunction with other measurements. In addition to continuous validation measurements at specific sites, essential support to high-latitude satellite data interpretation could be given by collecting together relevant ground-based satellite validation instrumentation and characterising related environmental variables. Particularly a co-designed, dedicated Arctic campaign cross-cutting atmospheric, soil and snow measurements would advance understanding of natural methane emission processes, suitable proxies and the added benefit of multi-satellite observations.

3.2 Methodological developments

3.2.1 Big-data assimilation technique

The number of GHG satellites is increasing and the number of useful atmospheric observations increases exponentially. It is critical to develop the assimilation techniques to be able to handle those big data. In the CarbonTracker models, we are currently using sequential assimilation due to mathematical assumption and methodology behind. Possible alternatives are, e.g., applying dimension reduction methods following e.g. Solonen et al. (2016), and parallelising the assimilation design by spliting the global domain to subregions (e.g. three latitudinal bands) and using data mining to select a meaningful number of observations for assimilation in each subregion.

In addition, powerful supercomputers have been developed, and can make use of high resolution models in the atmospheric inversions as well. This will enable an increase in spatial and temporal resolutions of the inversions. Also, combining Lagrangian transport modelling with the current global atmospheric transport model will reveal high resolution features in the transport patterns.

3.2.2 CCDAS-CH_4 assimilation technique

In this study, the atmospheric inversion system was used, which assimilated atmospheric CH_4 observations to infer fluxes. However, further development on assimilating e.g. land surface data informing on ecosystem or soil state, micrometeorological flux data, or economic statistics, and optimizing process-based model parameters at the same time (CCDAS system) will be useful. Some European projects are already aiming for such development for methane, and collaboration between research institutions could be strengthened.

3.2.3 Profile retrieval development for satellite observations

The recent success in applying dimension-reduction and Markov Chain Monte Carlo methods in the profile retrieval of methane from near-infrared spectra measured by ground-based Fourier Transform Spectrometers (Tukiainen et al., 2016; Karppinen et al., 2020) encourages for a further investigation on whether such methodologies are applicable to satellite retrievals of methane. Vertical profile information on the distribution of methane is highly important especially from source-sink estimation perspective, as described in Sect. 3.1.5.

3.2.4 Advancement of data-driven methodologies

Novel GHG satellites provide a wealth of data in terms of spatial resolution and coverage. While it is important to study the ingestion of these data in atmospheric inversion models, it is equally important to develop, in parallel, methodologies for data-driven source-sink estimation. For CO_2, this has been piloted by Hakkarainen et al. (2016) who introduced the concept of XCO_2 anomalies from OCO-2 data and have applied this concept especially for the space-based detection of anthropogenic emission sources. Studies on an equivalent development for methane emission signatures should be undertaken.

3.3 Roadmap

This project has contributed to an improved understanding on the northern latitude methane emissions, particularly in quantifying the emissions during the soil freezing period and improving the consideration of the freezing period in inverse modelling. First steps have been taken in the application of multi-satellite data but vast potential remains in the utilization of simultaneous observations of different environmental variables. For an increased knowledge on the remote Arctic region that is most comprehensively observed using satellites, further progress in the interpretation and use of the existing and emerging satellite data is necessary. In this framework, the upcoming initiative on Esa-Nasa collaboration on permafrost and methane is extremely timely.

While all developments outlined in Sect. 3.1–3.2 are considered important next steps for further knowledge on Arctic methane emissions, primary attention should be given to the following research questions:

- What is the seasonal cycle of the Northern latitude methane emissions in the permafrost and non-permafrost regions?
- What is the role of environmental drivers, such as snow cover, soil temperature and hydrology, in driving biospheric emissions, their seasonal cycle and trends?
- How are the anthropogenic emissions developing at the high Northern latitudes and how to best distinguish these emission signatures from space?
- What tracers and proxies are the most valuable for methane source attribution, either to facilitate direct observation or to inform inverse modelling?
- Can rapid emission changes (due to e.g. abrupt thaw) be identified?

These science questions could directly be used to initiate further research work in the path towards an encompassing view and understanding of Arctic methane in the changing climate.

4 Summary and Discussion

The MethEO project aimed to identify the magnitude of biospheric CH_4 emissions in northern high latitudes (NHL) and globally, provide trend analysis of the methane emissions during recent decades, and identify changes in the annual cycle of CH_4 emissions, focusing on soil freeze/thaw periods. EO data of global soil F/T estimates from ESA Soil Moisture and Ocean Salinity Mission (SMOS), and retrievals of atmospheric methane obtained from GOSAT and S5P-TROPOMI satellites were used in this work together with atmospheric inversion modelling of methane emissions (Carbon Tracker Europe - CH_4)

The emissions were estimated using both ground-based and satellite column CH_4 observations and different inversion set-ups. The global total emissions are estimated to be 526-561 ± 72 Tg CH_4 yr^{-1}, varying little among the different approaches. The share of global biospheric to total emissions vary between 24 - 30 % among the inversions, depending on underlying prior and observations assimilated.

The estimated biospheric emissions for regions around two major NHL wetlands were 5.3 to 11.1 Tg CH_4 yr^{-1} for Western Siberian Lowland (WSL) and 3.2 to 5.6 Tg CH_4 yr^{-1} for Canadian Hudson Bay Lowlands (HBL), and the estimates were within the uncertainty range of the previous studies (Peltola et al., 2019). Emissions from the intensive case study region were 0.3 to 0.8 Tg CH_4 yr^{-1}. The surface inversions show nice convergence among their posterior estimates for the HBL and NHL soil freezing period emissions. Comparison against flux data from the intensive study region and other sites showed that the seasonal cycle of the measured fluxes and modelled fluxes agree well. However, the results for the HBL region and the NHL soil freezing period emissions from the inversion assimilating GOSAT data was approximately two to three times higher than those from other inversion setups. Based on the analysis of the posterior atmospheric CH_4 at in-situ stations, we suspect that the NHL biospheric emission estimates from the GOSAT inversion may be overestimated.

During the soil freezing period, we found that the NHL methane fluxes decrease when the air and soil temperatures approach zero and are finally retained in low winter level. We found a good correlation between methane fluxes and length of the freezing period, indicating that methane emissions increase when the length of the freezing period increases. Evaluation against in situ CH_4 flux and atmospheric CH_4 observations showed that using reliable prior biospheric fluxes improves spatial and temporal distribution of the NHL cold season CH_4 fluxes from the atmospheric inversions. The implementation of SMOS F/T data reduced NHL emissions by 0.41 Tg CH_4 yr^{-1}, where the reduction mostly occurred in WSL winter. The results significantly improved the agreement with the atmospheric CH_4 observations throughout the years (2010-2017), indicating the importance of properly including soil conditions in modelling NHL winter CH_4 emissions.

The application of the GOSAT and TROPOMI XCH_4 showed both potential and challenges of those data to be used in the atmospheric inversions. The average annual global total emissions agreed well with the inversion estimates using surface in-situ atmospheric CH_4 data, and the posterior XCH_4 values agreed well with the assimilated XCH_4 data. A major difficulty resides on the methods to take the retrieval biases into account. The inversion using TROPOMI XCH_4 data resulted in smaller CH_4 emissions globally compared to other setups, which is possibly affected by biases in the retrieval data. In addition, the estimated northern European monthly emissions showed a lower summer maximum, and no clear month-to-month differences during summer in the TROPOMI inversion. This may be due to TROPOMI XCH_4 seasonal bias, which has been detected against TCCON (positively biased in winter and the differences decrease towards autumn and become negatively biased in the end of autumn). This indicates that the estimated seasonal cycle amplitude is possibly underestimated. The latitudinal bias in the GOSAT data needs to be further analysed. Although some biases were removed before inversion, the evaluation of posterior atmospheric CH_4 at inversion-independent in situ stations showed strong positive biases in the NH in the GOSAT inversion.

The estimated average trend over 2000-2018 from CTE-CH_4 inversions show an increase in global total emissions, mostly associated with the increase in anthropogenic emissions, while the trends in global total biospheric emissions are weak and appear positive according to the GOSAT inversion and negative according to surface inversions. In two regions in northern Siberia, the start date of the soil freezing period has a significant increasing trend, while the end date remains relatively unchanged. This implies that the total length of the soil freezing period becomes shorter. For the purpose of this study, the start and end date of the freezing period within a larger region was defined based on thresholds. For the start date 2% and for the end date 80% of the overall pixels were required to be frozen (see Section 2.3.2 for more details). The increasing trend in the start date indicates that the start of the soil freezing is delayed specifically at high latitude and/or high elevation regions – those areas where the thermal winter begins at earliest. Similarly, absence of changes in the end date would suggest that similar delays are not detected for areas where thermal winter tend to start at later date. Further and more detailed investigations are needed to study the reason behind this behaviour. The trends in freezing period emissions in those two regions in Siberia are mostly insignificant and indicate both positive and negative tendencies depending on regions and inversion set-ups. Thus, the existence of a significant emission trend during the soil freezing period remains inconclusive in light of the current results, and needs further investigations, examining all northern latitude results and environmental drivers of the emissions in detail.

5 References

Arndt KA, Oechel WC, Goodrich JP, Bailey BA Kalhori A., Hashemi J., Sweeney C. Zona D. Sensitivity of Methane Emissions to Later Soil Freezing in Arctic Tundra Ecosystems https://doi.org/10.1029/2019JG005242, 2019

Buldovicz et al., 2018 Cryovolcanism on the Earth: Origin of a Spectacular Crater in the Yamal Peninsula (Russia)

Center for International Earth Science Information Network - CIESIN - Columbia University. 2018. Gridded Population of the World, Version 4 (GPWv4): Population Count, Revision 11. Palisades, NY: NASA Socioeconomic Data and Applications Center (SEDAC). https://doi.org/10.7927/H4JW8BX5. Accessed 19 March 2020.

Crisp et al.: A CONSTELLATION ARCHITECTURE FOR MONITORING CARBON DIOXIDE AND METHANE FROM SPACE. Prepared by the CEOS Atmospheric Composition Virtual Constellation Greenhouse Gas TeamVersion 1.0 – 8 October 2018

Detmers, R.: System Verification Report (SVR) GHG-CCI Phase 2 CRDP#3 for sub-system CH4_GOS_SRFP version 3, http://www.esa-ghg-cci.org/?q=webfm_send/365, 2016a.

Detmers, R.: System Verification Report (SVR) GHG-CCI Phase 2 CRDP#3 for sub-system CH4_GOS_SRPR version 3, http://www.esa-ghg-cci.org/?q=webfm_send/364, 2016b.

Doxsey-Whitfield, E., MacManus, K., Adamo, S. B., Pistolesi, L., Squires, J., Borkovska, O. and Baptista, S. R.: Taking Advantage of the Improved Availability of Census Data: A First Look at the Gridded Population of the World, Version 4, Papers in Applied Geography, 1(3), 226–234, doi:10.1080/23754931.2015.1014272, 2015Kizyakov et al., 2017 Geomorphological conditions of the gas-emission crater and its dynamics in Central Yamal

Frey, M., Sha, M.K., Hase, F., Kiel, M., Blumenstock, T., Harig, R., Surawicz, G., Deutscher, N.M., Shiomi, K., Franklin, J.E. and Bosch, H., 2019. Building the COllaborative Carbon Column Observing Network (COCCON): long-term stability and ensemble performance of the EM27/SUN Fourier transform spectrometer.
Hakkarainen, J., Ialongo, I. and Tamminen, J., 2016. Direct space-based observations of anthropogenic CO2 emission areas from OCO-2. *Geophysical Research Letters*, *43*(21), pp.11-400.

Karppinen, T., Lamminpää, O., Tukiainen, S., Kivi, R., Heikkinen, P., Hatakka, J., Laine, M., Chen, H., Lindqvist, H. and Tamminen, J., 2020. Vertical Distribution of Arctic Methane in 2009–2018 Using Ground-Based Remote Sensing. *Remote Sensing*, *12*(6), p.917.

Kivi, R. and Heikkinen, P., 2016. Fourier transform spectrometer measurements of column CO2 at Sodankylä, Finland. *Geoscientific Instrumentation, Methods and Data Systems*, *5*(2), pp.271-279.

Kivimäki, E., Lindqvist, H., Hakkarainen, J., Laine, M., Sussmann, R., Tsuruta, A., Detmers, R., Deutscher, N.M., Dlugokencky, E.J., Hase, F. and Hasekamp, O., 2019. Evaluation and Analysis of the Seasonal Cycle and Variability of the Trend from GOSAT Methane Retrievals. *Remote Sensing*, *11*(7), p.882.

Krol, M., Houweling, S., Bregman, B., van den Broek, M., Segers, A., van Velthoven, P., Peters, W., Dentener, F., and Bergamaschi, P.: The two-way nested global chemistry-transport zoom model TM5: algorithm and applications, Atmos. Chem. Phys., 5, 417–432, https://doi.org/10.5194/acp-5-417-2005, 2005.
Olsen et al., 2017 https://www.atmos-meas-tech.net/10/3697/2017/amt-10-3697-2017.pdf

Ostler, A., Sussmann, R., Patra, P. K., Houweling, S., De Bruine, M., Stiller, G. P., Haenel, F. J., Plieninger, J., Bousquet, P., Yin, Y., Saunois, M., Walker, K. A., Deutscher, N. M., Griffith, D. W. T., Blumenstock, T., Hase, F., Warneke, T., Wang, Z., Kivi, R., and Robinson, J.: Evaluation of column-averaged methane in models and TCCON with a focus on the stratosphere, Atmos. Meas. Tech., 9, 4843–4859, https://doi.org/10.5194/amt-9-4843-2016, 2016.

Peltola, O., Vesala, T., Gao, Y., Räty, O., Alekseychik, P., Aurela, M., Chojnicki, B., Desai, A. R., Dolman, A. J., Euskirchen, E. S., Friborg, T., Göckede, M., Helbig, M., Humphreys, E., Jackson, R. B., Jocher, G., Joos, F., Klatt, J., Knox, S. H., Kowalska, N., Kutzbach, L., Lienert, S., Lohila, A., Mammarella, I., Nadeau, D. F., Nilsson, M. B., Oechel, W. C., Peichl, M., Pypker, T., Quinton, W., Rinne, J., Sachs, T., Samson, M., Schmid, H. P., Sonnentag, O., Wille, C., Zona, D. and Aalto, T.: Monthly gridded data product of northern wetland methane emissions based on upscaling eddy covariance observations, Earth System Science Data, 11(3), 1263–1289, doi:https://doi.org/10.5194/essd-11-1263-2019, 2019.

Poulter, B., Bousquet, P., Canadell, J. G., Ciais, P., Peregon, A., Saunois, M., Arora, V. K., Beerling, D. J., Brovkin, V., Jones, C. D., Joos, F., Gedney, N., Ito, A., Kleinen, T., Koven, C. D., McDonald, K., Melton, J. R., Peng, C., Peng, S., Prigent, C., Schroeder, R., Riley, W. J., Saito, M., Spahni, R., Tian, H., Taylor, L., Viovy, N., Wilton, D., Wiltshire, A., Xu, X., Zhang, B., Zhang, Z. and Zhu, Q.: Global wetland contribution to 2000–2012 atmospheric methane growth rate dynamics, Environmental Research Letters, 12(9), 094013, doi:10.1088/1748-9326/aa8391, 2017.

Rayner, P. J., M. Scholze, W. Knorr, T. Kaminski, R. Giering, and H. Widmann (2005), Two decades of terrestrial carbon fluxes from a carbon cycle data assimilation system (CCDAS), Global Biogeochem. Cycles, 19, GB2026, doi:10.1029/2004GB002254.

Saunois, M., Stavert, A. R., Poulter, B., Bousquet, P., Canadell, J. G., Jackson, R. B., Raymond, P. A., Dlugokencky, E. J., Houweling, S., Patra, P. K., Ciais, P., Arora, V. K., Bastviken, D., Bergamaschi, P., Blake, D. R., Brailsford, G., Bruhwiler, L., Carlson, K. M., Carrol, M., Castaldi, S., Chandra, N., Crevoisier, C., Crill, P. M., Covey, K., Curry, C. L., Etiope, G., Frankenberg, C., Gedney, N., Hegglin, M. I., Höglund-Isakson, L., Hugelius, G., Ishizawa, M., Ito, A., Janssens-Maenhout, G., Jensen, K. M., Joos, F., Kleinen, T., Krummel, P. B., Langenfelds, R. L., Laruelle, G. G., Liu, L., Machida, T., Maksyutov, S., McDonald, K. C., McNorton, J., Miller, P. A., Melton, J. R., Morino, I., Müller, J., Murgia-Flores, F., Naik, V., Niwa, Y., Noce, S., O'Doherty, S., Parker, R. J., Peng, C., Peng, S., Peters, G. P., Prigent, C., Prinn, R., Ramonet, M., Regnier, P., Riley, W. J., Rosentreter, J. A., Segers, A., Simpson, I. J., Shi, H., Smith, S. J., Steele, P. L., Thornton, B. F., Tian, H., Tohjima, Y., Tubiello, F. N., Tsuruta, A., Viovy, N., Voulgarakis, A., Weber, T. S., Weele, M. van, Werf, G. R. van der, Weiss, R. F., Worthy, D., Wunch, D., Yin, Y., Yoshida, Y., Zhang, W., Zhang, Z., Zhao, Y., Zheng, B., Zhu, Q., Zhu, Q. and Zhuang, Q.: The Global Methane Budget 2000-2017, Earth System Science Data Discussions, 1–138, doi:https://doi.org/10.5194/essd-2019-128, 2019.

Solonen, A., Cui, T., Hakkarainen, J. and Marzouk, Y.: On dimension reduction in Gaussian filters, Inverse Problems, 32(4), 045003, doi:10.1088/0266-5611/32/4/045003, 2016.

Stocker, B. D., Spahni, R. and Joos, F.: DYPTOP: a cost-efficient TOPMODEL implementation to simulate sub-grid spatio-temporal dynamics of global wetlands and peatlands, Geosci. Model Dev., 7(6), 3089–3110, doi:10.5194/gmd-7-3089-2014, 2014.

Wunch, D., Toon, G.C., Blavier, J.F.L., Washenfelder, R.A., Notholt, J., Connor, B.J., Griffith, D.W., Sherlock, V. and Wennberg, P.O., 2011. The total carbon column observing network. *Philosophical Transactions of the Royal Society A: Mathematical, Physical and Engineering Sciences*, *369*(1943), pp.2087-2112.

Yoshida, Y., Kikuchi, N., Morino, I., Uchino, O., Oshchepkov, S., Bril, A., Saeki, T., Schutgens, N., Toon, G., Wunch, D., Roehl, C. M., Wennberg, P. O., Griffith, D. W. T., Deutscher, N. M., Warneke, T., Notholt, J., Robinson, J., Sherlock, V., Connor, B., Rettinger, M., Sussmann, R., Ahonen, P., Heikkinen, P., Kyro, E., Mendonca, J., Strong, K., Hase, F., Dohe, S., and Yokota, T.: Improvement of the retrieval algorithm for GOSAT SWIR XCO2 and XCH4 and their validation using TCCON data, Atmos. Meas. Tech., 6, 1533–1547, 2013.

Zona D, Gioli B, Commane R, Lindaas J, Wofsy SC, Miller CE, Dinardo SJ, Dengel S, Sweeney C, Karion A, Chang RYW, Henderson JM, Murphy PC, Goodrich JP, Moreaux V, Liljedahl A, Watts JD, Kimball JS, Lipson DA, Oechel WC. Proceedings of the National Academy of Sciences 113 (1) 40-45; DOI: 10.1073/pnas.1516017113, 2016